

# Bioinspired Physico-Chemical Surface Modifications for the Development of Advanced Retentive Systems

Eda Dzinovic, Lauren Clark, Niktash Keyhani, Nora Al Morhiby, Paul Byford, Siyang Wang, Sara Gamea, Kenneth Chu, Elizabeth Wnuk, Yu Liu, Nicole Rosik, Finn Giuliani, Nicola M. Pugno, Zhenyu J. Zhang, Owen Addison, and Sherif Elsharkawy\*

A major aspiration in advanced materials is to create artificial adhesive surfaces for wearable medical devices to meet the demands of the body's challenging settings and dynamics. For instance, dentures replace missing teeth and operate within the oral cavity, where an interplay between forces, muscles, saliva, and roughness of mucosa undermine their ability to grip oral tissues. Consequently, the lack of effective retentive strategies represents a source of dissatisfaction for denture wearers globally. Nature is rich in examples that employ physical and chemical adhesive strategies to optimize interfacial forces in dry and wet environments. Here, keratin-coated octopus-like suction cups are presented at the micro- and macroscale to improve the retention of rigid poly(methyl methacrylate). Microtopographies are obtained using two-photon polymerization and maskless lithography, while denture prototypes with macrotopographies are derived via digital light processing 3D printing. Results suggest that microtopographies and keratin-coated surfaces sustain higher maximum adhesion stress than the non-topographical and non-coated surfaces in moist environments, where retention is typically lacking. Proof-of-concept dentures demonstrate higher maximum detachment forces than conventional dentures with and without denture adhesive within dry and wet environments. This interdisciplinary research highlights the potential application of a nature-inspired physico-chemical approach in the next generation of complete dentures.

## 1. Introduction

Edentulism, or the absence of natural teeth, is a complex and irreversible condition that has been an overlooked aspect of overall health and well-being.<sup>[1,2]</sup> Contemporary awareness of edentulism has increased, with many countries now monitoring it as the “ultimate indicator of disease burden for oral health”, affecting more than 350 million people worldwide and impacting both healthcare services and the quality of life.<sup>[3–6]</sup> The two most common non-communicable diseases in humans, dental caries and periodontitis contribute to progressive tooth loss alongside unequal access to dental services.<sup>[6–10]</sup>

Poly(methyl methacrylate) (PMMA or acrylic) complete dentures are the most common and cost-effective treatment solution for edentulism. The success of dentures relies on precise coverage of the mucosa to achieve retention. However, the hydrophobic nature and poor adhesion of PMMA to oral

E. Dzinovic, L. Clark, N. Keyhani, N. Al Morhiby, S. Gamea, K. Chu, E. Wnuk, O. Addison, S. Elsharkawy  
Centre for Oral, Clinical & Translational Sciences  
Faculty of Dentistry  
Oral & Craniofacial Sciences  
King's College London  
London SE1 9RT, UK  
E-mail: [sherif.elsharkawy@kcl.ac.uk](mailto:sherif.elsharkawy@kcl.ac.uk)  
P. Byford, O. Addison, S. Elsharkawy  
Dental Directorate  
Guys & St. Thomas' NHS Trust  
London SE1 9RT, UK

 The ORCID identification number(s) for the author(s) of this article can be found under <https://doi.org/10.1002/admt.202400928>

© 2024 The Author(s). Advanced Materials Technologies published by Wiley-VCH GmbH. This is an open access article under the terms of the [Creative Commons Attribution](#) License, which permits use, distribution and reproduction in any medium, provided the original work is properly cited.

DOI: 10.1002/admt.202400928

S. Wang, F. Giuliani  
Department of Materials  
Royal School of Mines  
Imperial College London  
London SW7 2AZ, UK  
Y. Liu, N. Rosik, Z. J. Zhang  
School of Chemical Engineering  
University of Birmingham  
Birmingham B15 2TT, UK  
N. M. Pugno  
Laboratory for Bioinspired, Bionic, Nano, Meta Materials and Mechanics  
Department of Civil  
Environmental and Mechanical Engineering  
University of Trento  
Trento 38123, Italy  
N. M. Pugno  
School of Engineering and Materials Science  
Queen Mary University of London  
London E1 4NS, UK

tissues, coupled with the dynamic conditions in the mouth, often result in inadequate denture retention.<sup>[11–16]</sup> Denture adhesive creams are chemical adjuncts typically used for improperly fitting dentures.<sup>[17,18]</sup> Adhesive creams contain macromolecules, such as methylcellulose, which have a natural tendency to absorb water from saliva. The absorption leads to the formation of hydrogen bonds within the adhesive, thereby increasing its viscosity and improving the adhesion between the denture and mucosa.<sup>[19]</sup> Nevertheless, many patients reject adhesives as they find them unhygienic, difficult to remove, and prone to trigger gagging, nausea, and taste alteration.<sup>[16,20]</sup> To date, implants have been considered as a gold standard for improperly fitting dentures,<sup>[21,22]</sup> but insufficient bone support,<sup>[23]</sup> radio-and bisphosphonate therapy,<sup>[24–26]</sup> systemic diseases,<sup>[27]</sup> a wish to avoid surgery,<sup>[28]</sup> and out-of-pocket expenses<sup>[29]</sup> exclude the implants as a viable option. Given these challenges alongside the growing geriatric population, PMMA complete dentures will remain the primary treatment for edentulism in the foreseeable future.<sup>[6,30]</sup> Over the years, various methods have been attempted to improve denture retention, such as abrasion of the fitting surface to enhance wettability and hydrophilicity<sup>[31]</sup> or the introduction of large soft suction cups.<sup>[32–35]</sup> The abrasion technique resulted in poor reproducibility, dimensional variability, and inconsistent distribution of surface irregularities. Single suction cup dentures required merging two or more materials with different physical and chemical properties (i.e., flexible silicone and rigid PMMA), which not only amplified the chances of debonding, but also added more steps to the already lengthy denture fabrication process. As a result, none of these techniques have been widely adopted in clinical practice.

In contrast to the challenges encountered in materials science, achieving retention in nature appears to be a straightforward effort. Nature is rich in examples that employ morphology and chemical products to optimize interfacial forces in dry and wet environments. For instance, multiscale topographies in the form of microneedles, fibrils, hexagons, or suction cups amplify the physical interaction with the substrate.<sup>[36]</sup> The adhesion system of *Octopus vulgaris* has become one of the most studied models due to its ability to grip both dry and wet surfaces and unique architecture, which includes a dome-shaped protuberance and an orifice.<sup>[37–41]</sup> Of note, flexible skin adhesives with micro-scale octopus-inspired suckers were already developed using conventional lithography. These adhesives resulted in strong and reversible adhesion in dry, moist, wet, and oily conditions.<sup>[42]</sup> However, conventional lithography could not harness the complex architecture of a suction cup, thus additional step (partial wetting) was employed to fabricate a protuberance. In another study, extruded microsuckers exhibited high pull-off adhesion forces in dry and wet environments. These microsuckers required multiple steps to generate protuberance, specifically liquid trapping and electrowetting techniques.<sup>[43]</sup> Recent research demonstrated enhanced adhesion of octopus-inspired 3D-printed buccal patches for drug delivery. Due to the need for drug incorporation, these suction cups had large diameters of 11 mm, which made them unsuitable for various applications.<sup>[44]</sup> On the other hand, polymers, such as dopamine in mussels or keratin in gecko's toepad fibrils, improve energetic interactions

at interfaces and lead to higher detachment forces.<sup>[45]</sup> Specifically, keratin is considered one of the most crucial animal proteins due to its abundant presentation in hair, wool, fur, hard palate and gums, skin, nails, horns, and hooves.<sup>[46]</sup> Unlike other proteins, keratin's high cysteine content and a large number of robust disulfide bonds contribute to its intrinsic properties to self-assemble and form complex 3D structures resistant to common enzymes (pepsin and trypsin) and chemical hydrolysis in weak acids, alkaline solutions, and organic solvents.<sup>[47]</sup> Furthermore, bio- and cytocompatibility, non-immunogenicity, durability, stiffness, strength when present in thin layers, response to hydration, structural conservation across species, and inexpensive isolation make keratin a promising alternative biomaterial compared to synthetic polymers in denture adhesive creams.<sup>[46,48,49]</sup> Recent studies showed that keratin exhibits tunable mucoadhesiveness in gastric drug delivery systems,<sup>[50]</sup> high propensity to mucin,<sup>[51]</sup> wound healing effect,<sup>[48]</sup> osteoconductive properties,<sup>[52]</sup> and cell-binding potential,<sup>[53]</sup> allowing it to interact with natural tissues and express chemotactic properties.

Biomimetics, the concept of mimicking processes, objects, and products in nature, has emerged as a promising route to enhance the retention of biomaterials.<sup>[36,45]</sup> Recent advancements in micro- and macro 3D printing techniques, including two-photon polymerization, direct-write laser lithography, and digital light processing (DLP), enable structural mimicking of natural adhesive surfaces and their topographies. The high-throughput and submicrometric fabrication accuracy of two-photon polymerization and direct-write laser lithography enable consistent printing of multiple complex shapes in aspect ratios where the fundamental mechanisms of microtopographies remain unchanged, yet their broader application becomes more convenient.<sup>[36,45,54]</sup> Commercially available DLP 3D printers also enable shape complexity, precision, consistency, and rapid fabrication of macro structures from a single biocompatible material, making the final object/device readily applicable in practice.<sup>[54]</sup>

Using advanced printing techniques, we present the development of octopus-inspired topographies at various scales to serve as an innovative retentive system for traditional dental materials (**Figure 1A,B**). Our results indicate that direct-laser writing allows the fabrication of simple microtopographies, octopus holes (OH), which enhance the mucoadhesion of PMMA in moist conditions. Two-photon polymerization goes beyond the limitations of traditional lithography, enabling the production of complex structures with deep undercuts—octopus suckers (OS). Unlike conventional denture manufacturing, our DLP 3D printing integrates bioinspired retentive features into a single material, resulting in the fabrication of proof-of-concept dentures with highly characterized octopus-like macrotopographies. These suction cup dentures exhibit higher pull-off adhesion forces *ex vivo* versus conventional complete dentures with or without denture adhesive, both in dry and wet conditions. Alongside physical adhesion derived from topographies, we introduce a dimension of chemical adhesion. In this context, functionalization of hydrophobic PMMA with extracted hydrophilic biopolymer keratin does not only improve the hydrophilicity of PMMA, but also reveals a synergistic retentive effect with micro-scale PMMA-based octopi suckers in moist conditions.

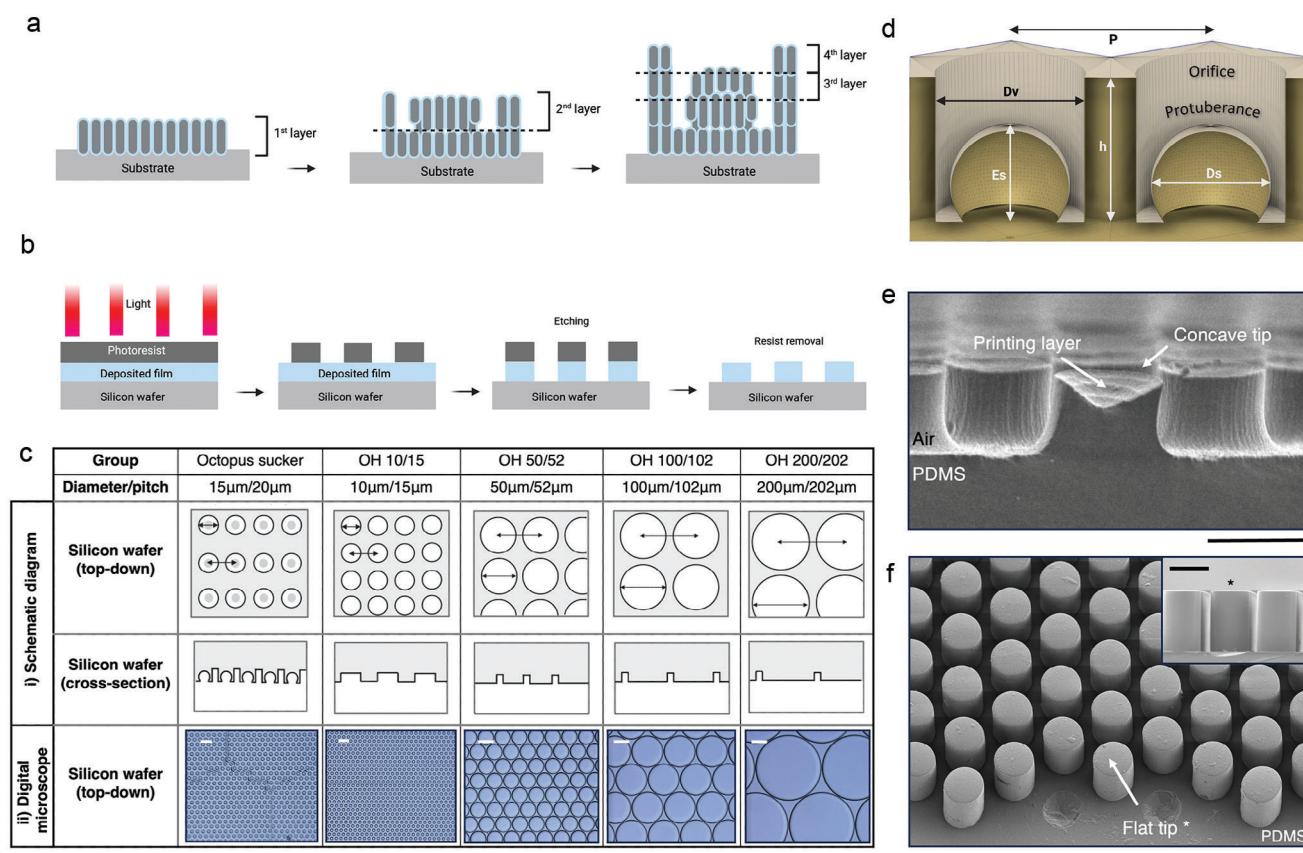


**Figure 1.** Fabrication of microtopographies, shapes, and structures. A) Fabrication of octopus-like topographies via 3D two-photon polymerization and B) direct-write laser lithography to generate octopi suckers (OS) and octopi holes (OH), respectively. C) Table summarizing the (i) schematic and (ii) microscopic (magnification  $\times 500$ ) outline of topographies laid out on a Si wafer. Scale bars, OS – 40  $\mu$ m, OH 10/15- 30  $\mu$ m, OH 50/52- 50  $\mu$ m, OH 100/102- 50  $\mu$ m, OH 200/202- 50  $\mu$ m. D) Cross-sectional view of an OS group with protuberance. Dimensions are as follows:  $h = 15 \mu\text{m}$ ,  $D_v = 15 \mu\text{m}$ ,  $D_s = 12 \mu\text{m}$ ,  $E_s = 9.6 \mu\text{m}$  (80% of sucker's height),  $P = 20 \mu\text{m}$ ,  $s = 5 \mu\text{m}$ . E) Cross-sectional SEM image of an OS group's negative PDMS with a concavity on the top of a cylinder ( $\times 2000$ ). Scale bar, 15  $\mu\text{m}$ . F) Top-down and cross-sectional view (inset) of an OH 10/15 group's negative PDMS shows a flat-tipped structure ( $\times 1200$ ). Scale bars, main image 20  $\mu\text{m}$ , inset 10  $\mu\text{m}$ .

## 2. Results and Discussion

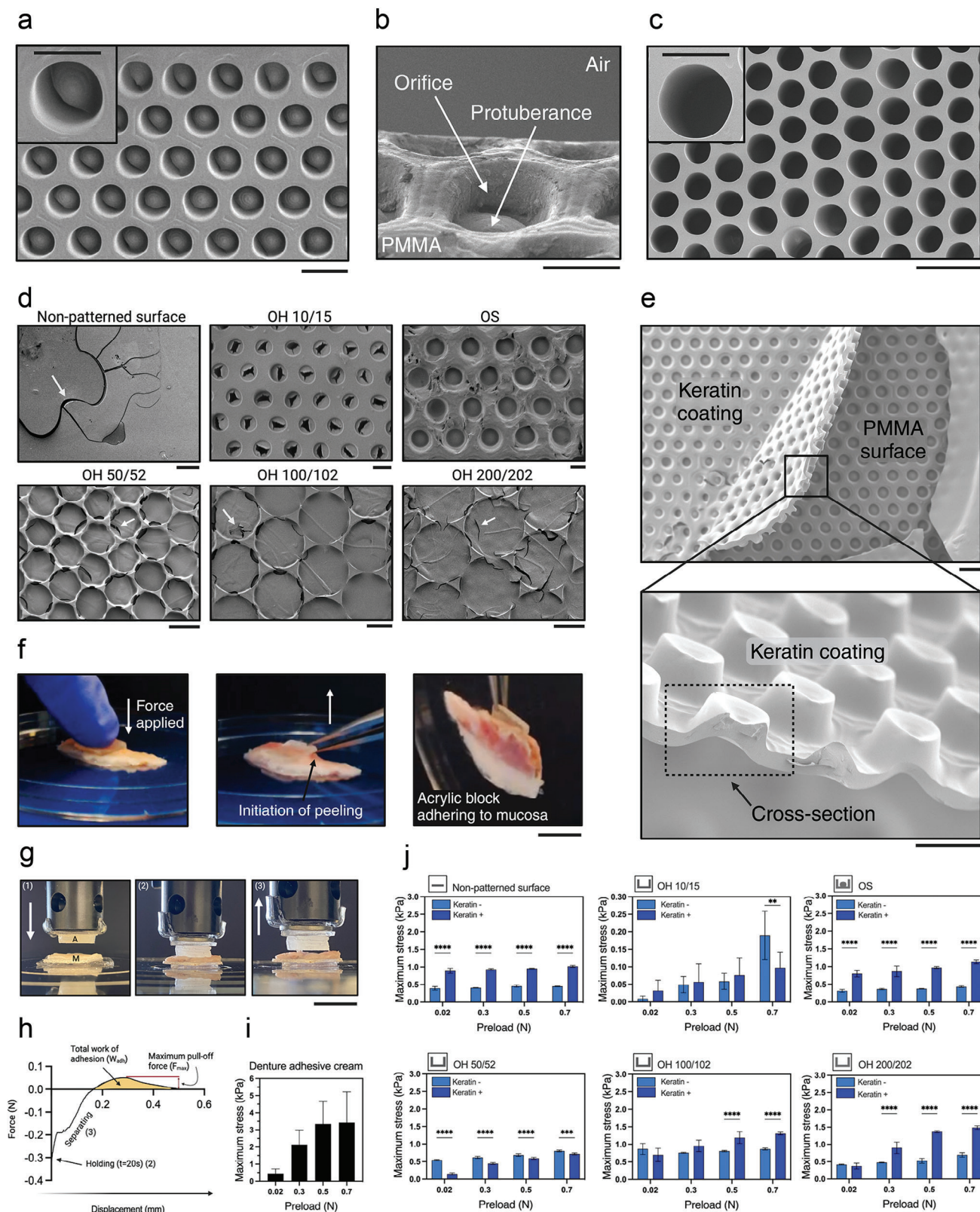
### 2.1. Fidelity of Replication

Silicon (Si) wafers contained two modifications of an octopus architecture; a range of simplified topographies – octopi holes (OH), and a more complex model – OS that comprised the orifice and the protuberance (Figure 1C,D). We employed the replica molding technique to fabricate negative PDMS molds (Figure S1, Supporting Information). The negative PDMS molds represented the inverted patterns of the original Si wafer and were obtained to transfer topographies from the Si wafer to PMMA.

Inspection of negative molds using a digital light microscope unveiled that the geometry of our main OS group was replicated in PDMS, overcoming the challenges posed by the complex architecture and the low scalability of the Si wafer design (Figure 1E; Figure S2a, Supporting Information). Dimension-wise, OH 10/15 was closest to the OS, except that it did not contain the protuberance (Figure 1F). Due to the larger diameter, OS had a lower density of topographies (285/cm<sup>2</sup>) compared to the OH 10/15 (400/cm<sup>2</sup>) (Figure S1, Supporting Infor-

mation). Top-down observation of OH 50/52, OH 100/102, and OH 200/202 PDMS molds demonstrated densely populated topographies, with 192, 98, and 50 holes per cm<sup>2</sup>, respectively. Each topography was separated by a thin wall of PDMS measuring 2  $\mu$ m (Figure S2c–e, Supporting Information). Conversely, OS and OH 10/15 had wider separating walls (5  $\mu$ m) between two adjacent holes relative to other OH groups. Cross-sectional observation with scanning electron microscope (SEM) implied that the vertical dimensions of OS (Figure 1E) and OH PDMS groups (Figure 1F) were not altered upon peeling.

After transferring topographies from PDMS to PMMA (Figure S3a, Supporting Information), SEM showed an accurate replication of our main OS and OH 10/15 groups in hard PMMA, despite OS's complex structure with severe undercuts and protuberance, and OH's densely populated topographies (Figure 2A–C). This may be due to the thick separating walls (5  $\mu$ m) between their topographies, which contributed to high resistance and defect reduction. Other OH acrylic blocks, such as OH 50/52, OH 100/102, and OH 200/202 groups, had lower structural fidelity and did not fully attain the aspired replication, resulting in the presence of incomplete holes (Figure S3b–d, Supporting



Information). These defects may be attributed to the thinner separating walls (2  $\mu\text{m}$ ) between the topographies, as well as the polymerization shrinkage of PMMA, which occurs during curing. Despite efforts to minimize the shrinkage rate by mixing the PMMA in recommended ratios,<sup>[55]</sup> we concluded that maintaining the integrity of topographies with extremely thin separating walls (< 5  $\mu\text{m}$ ) is challenging using the implemented replication technique.

We also examined the surface of PMMA blocks after keratin coating (Figure S4a, Supporting Information). Keratin was present on the surface of acrylic blocks, inside and around the entrances of topographies due to the PMMA's potential to adsorb proteins (Figure 2D; Figure S5, Supporting Information).<sup>[56,57]</sup> Prior to coating, keratin was in a dispersed state without distinct structural organization, as confirmed by atomic force microscopy (AFM) (Figure S4b, Supporting Information). AFM images showed a relatively smooth surface, with no significant roughness, indicating that the keratin is present as individual protein molecules or small aggregates in solution. Upon drying, the keratin underwent a self-assembly process, which resulted in the formation of a more structured coating. This process significantly increased the surface roughness, as shown in the post-drying AFM images (Figure S4c, Supporting Information), with certain areas becoming higher relative to others. This finding suggests that the keratin self-assembles into layer, likely due to interactions between cysteine residues and the reconstruction of disulfide bonds. Discontinuities and delamination were observed in the keratin layer due to the high-vacuum sputter coating performed before SEM imaging (Figure 2D). In the central regions of the blocks, the keratin layer was sufficiently thin (< 10  $\mu\text{m}$ ), precisely conforming to the shape of topographies (Figure 2E). In contrast, the peripheral regions of the coating were thicker, although their measurements remained below 10  $\mu\text{m}$ . Minor variations in thickness were observed between the coating on the surface and keratin parts extending into the topographies, with thicknesses of  $2.3 \pm 0.5 \mu\text{m}$  and  $5.3 \pm 1.7 \mu\text{m}$ , respectively. The higher variations in the thickness of the keratin coating inside the topographies may be attributed to different areas where cross-sections were made (Figure 2E).

## 2.2. Static Water Contact Angle (WCA)

To achieve the relevant retention, the fitting surface of a denture needs to be wetted to some extent. However, due to the PMMA's hydrophobic nature and low surface energy, wetting of

the denture base is challenging.<sup>[58]</sup> Literature suggests that topographies can alter the surface properties of a material, increasing its hydrophobicity which manifests in high contact angle values.<sup>[59]</sup> To preserve the retentive effect of topographies and prevent topography-induced low surface energy, we functionalized PMMA with keratin extracted from sheep's wool. Next, we compared the surface properties of PMMA blocks after both physical (topographies) and chemical (keratin) modifications by measuring static WCA ( $N = 3$ ).

Following physical alteration, groups OS, OH 10/15, and OH 50/52 demonstrated WCA values of  $22.3 \pm 0.5^\circ$ ,  $23.8 \pm 2.6^\circ$ , and  $21.16 \pm 1.3^\circ$ , respectively, thereby exhibiting significantly higher ( $P < 0.0001$ ) values than those of flat, non-patterned group ( $\theta = 15.5 \pm 1.6^\circ$ ) (Figure S6a,b, Supporting Information). We found a direct relationship between the WCA and the density of topographies on the acrylic blocks, i.e., the higher the density of the topographies, the larger the WCA. OH 10/15 had the largest number of topographies (400/cm<sup>2</sup>), thus the greatest WCA ( $\theta = 23.8 \pm 2.6^\circ$ ), which was followed by OS ( $\theta = 22.3 \pm 0.5^\circ$ ; 285/cm<sup>2</sup>) and OH 50/52 ( $\theta = 21.2 \pm 1.3^\circ$ ; 192/cm<sup>2</sup>). After 60 min, all WCAs decreased, yet the groups with the highest density of topographies (OS, OH 10/15, and OH 50/52) maintained the largest WCA values.

After keratin coating, OS demonstrated the largest initial WCA value ( $\theta = 15.1 \pm 1.1^\circ$ ) but without significant differences compared to other groups (Figure S6a,b, Supporting Information). After 60 min, WCAs on OH 50/52, OH 100/102, and OH 200/202 could not be measured, whereas OS underwent the minimal transformation from  $\theta = 15.1 \pm 1.1^\circ$  ( $t = 1 \text{ min}$ ) to  $\theta = 10.8 \pm 0.1^\circ$  ( $t = 60 \text{ min}$ ). The shift in the WCA values and the surface properties from hydrophobic to hydrophilic after functionalization with polymer is a common finding in the literature.<sup>[59–61]</sup> For instance, on non-coated patterned surfaces, the hydrophobicity of a material increases due to the surface roughness imposed by the presence of microtopographies. Upon wetting, the droplet sits on apical parts of topographies while air remains entrapped in the interstitial volumes underneath, resulting in the establishment of hydrophobic surface.<sup>[59]</sup> Addition of keratin coating resulted in the perturbations to the roughness-induced hydrophobicity which manifested in increased wettability and the smaller WCA values.<sup>[59]</sup> Smaller WCAs could be due to the high content of amine and carboxylic groups within the keratin. These functional groups interact with water molecules, increasing the surface energy of the substrate and demonstrating surfactant-like properties.<sup>[62,63]</sup> To confirm that keratin behaves like surfactant

**Figure 2.** Fidelity of replication and adhesion profiles for acrylic blocks with/without topographies and keratin. A) Top-down SEM image of an OS acrylic block showing multiple suction cups. Scale bars, main image 25  $\mu\text{m}$ , inset 15  $\mu\text{m}$ . B) Tilted perspective reveals true replication of orifice and protuberance (indicated with the arrows). Scale bar, 7  $\mu\text{m}$ . C) A top-down SEM image of OH 10/15 acrylic block comprising an empty hole without protuberance. Scale bars, main image 30  $\mu\text{m}$ , inset 10  $\mu\text{m}$ . D) Surfaces of selected topographies coated with keratin and observed under SEM. Arrows indicate the cracks in keratin coating. Scale bars, non-patterned surface 100  $\mu\text{m}$ , OH 10/15 10  $\mu\text{m}$ , OS 15  $\mu\text{m}$ , OH 50/52 50  $\mu\text{m}$ , OH 100/102 50  $\mu\text{m}$ , OH 200/202 100  $\mu\text{m}$ . E) A micrometer-thin layer of keratin coating formed on the surface of the OS PMMA block and conformed to the shape of the topographies. Scale bars, low magnification (x350) 20  $\mu\text{m}$ , high magnification (x2200) 10  $\mu\text{m}$ . F) Qualitative adhesion test in a moist environment shows prolonged contact between mucosa explant and keratin-coated acrylic block after initial peeling. Scale bar, 1 cm. G) Setup for a pull-off adhesion test where the acrylic block (A) is mounted on the moving crosshead, and mucosa (M) is glued onto a fixed platform of the machine – stage 1. The process involves bringing the acrylic block into a contact with the mucosa until the desired preload is achieved, holding for 20 s – stage 2, and then initiating retraction – stage 3. Scale bar, 5 mm. H) The force-displacement curve obtained during the separation process is analyzed to determine maximum detachment force ( $F_{\text{max}}$ ) and total work of adhesion ( $W_{\text{adh}}$ ). J) Adhesion profiles of non-coated (keratin-) and keratin-coated (keratin+) acrylic blocks, and I) commercial denture adhesive. Error bars in the graphs represent standard deviations for the samples ( $N = 20$ ). Statistics were performed using a two-way ANOVA with a Šidák's post-test, \* $p < 0.05$ , \*\* $p < 0.01$ , \*\*\* $p < 0.001$ , \*\*\*\* $p < 0.0001$ .

and increases the surface energy, we compared its effect on WCA to a commonly used surfactant, sodium dodecyl sulfate (SDS), in combinations as follows: (1) distilled water on acrylic; (2) distilled water with SDS on acrylic; and (3) distilled water on a keratin-coated acrylic. This resulted in WCA values of  $\theta = 15.6 \pm 0.9^\circ$ ,  $\theta = 9.8 \pm 1.7^\circ$ , and  $\theta = 11.6 \pm 1^\circ$ , respectively (Figure S6c, Supporting Information). After 40 min, the WCA on the non-coated acrylic surface was still visible ( $\theta = 9.7 \pm 1.7^\circ$ ), whereas other WCAs could not be measured. Our findings suggest that keratin enhances the surface energy of an acrylic surface, regardless of the presence or dimensions of topographies.

Alternatively, the hydrophilicity of keratin could be attributed to its negative charge when dissolved in a pH of 7, which was the adjusted pH for the keratin extraction and dissolution in our experiment. This negative charge causes keratin molecules to repel each other, leading to fewer hydrogen bonding sites. As a result, spaces within the keratin matrix facilitate the water penetration and lead to small WCAs.<sup>[64–66]</sup>

### 2.3. Qualitative Adhesion Test

A qualitative pull-off adhesion test was performed to approximate the mixed mode failure of the interface between denture and mucosa encountered clinically. This involved assessing the failure of both keratin-coated and non-coated, non-patterned acrylic blocks on the keratinized mucosa. For this purpose, we created two different situations: moist condition (where a subtle level of humidity was arising from the mucosa explant) and wet environment (where  $\approx 95\%$  of the mucosa explant was covered with distilled water). Keratin-coated acrylic blocks remained bonded to the mucosa in a moist environment, subsequently withstanding the attempts to break the established interface (Figure 2F; Movie S1, Supporting Information). On the other hand, non-coated acrylic blocks did not adhere to the mucosa as effectively as coated acrylic, resulting in swift detachment (Movie S2, Supporting Information). Qualitatively enhanced adhesion of a keratin-coated, non-patterned acrylic to the keratinized mucosa could be attributed to their chemical compatibility. Specifically, keratin comprises cysteine, a principal amino acid in nature that mediates the formation of covalent, disulfide bonds.<sup>[67,68]</sup> Therefore, it is plausible that the thiol groups within the cysteine-rich keratin establish disulfide bonds with thiol groups of keratins from the mucosa, leading to improved mucoadhesion.<sup>[68]</sup> Conversely, water in a wet environment presented a barrier between coated acrylic blocks and keratinized mucosa. Keratin is a hydrophilic biopolymer, that requires a certain level of water to achieve adhesion.<sup>[50]</sup> However, excessive hydration results in a low friction coefficient and the subsequent loss of mucoadhesion.<sup>[69–71]</sup> Due to the superior adhesion performance of keratin in a moist environment, all subsequent quantitative tests are conducted without the addition of water between the acrylic block and mucosa.

### 2.4. Quantitative Adhesion Test with Non-Coated Topographies

Each group underwent a pull-off adhesion test and mucoadhesion was evaluated across a range of preloads, including 0.02, 0.3, 0.5, and 0.7 N (Figure 2G,H). The idea of different preloads

was to (1) ensure close contact between samples, (2) create conditions for physical/chemical interactions, and (3) simulate the seating force that patients apply while placing their dentures. We assessed maximum detachment force to quantitatively determine the level of mucoadhesion and total work of adhesion as there can be a significant displacement between the block and mucosa prior to complete dislodgement/separation.

OH 100/102 performed the best across tested preloads, achieving maximum (adhesion) stress values ( $\sigma_{\max}$ ) of  $0.87 \pm 0.15$  kPa,  $0.76 \pm 0.013$  kPa,  $0.80 \pm 0.02$  kPa,  $0.86 \pm 0.03$  kPa, respectively, and surpassing the performance of the non-patterned surface. OH 50/52, OH 200/202, and OH 10/15 exhibited increased maximum stress values with higher preloads while OS displayed a monotonous trend (Figure 2J). Additionally, all groups significantly ( $P < 0.0001$ ) outperformed OH 10/15, demonstrating a tenfold increase in maximum stress values across all preloads. Apart from OH 100/102 and non-patterned control, the total work of adhesion was improved for all other groups when larger preloads were applied (Figure S7, Supporting Information). Conversely, the preload did not impact the maximum stress of non-coated acrylic samples. Additional experiments with the force plate confirmed the abovementioned findings of the large-scale tensile tester and indicated insensitivity to applied preloads (Figure S8a–c, Supporting Information). Only a denture adhesive cream demonstrated a preload-dependent behavior (Figure 2I; Figure S8b,c, Supporting Information). Quantitative adhesion test of non-coated topographies highlighted that larger OH groups attained higher maximum stress values than non-patterned surfaces and OS. For the OS group, it might be that its protuberance in the hard material at the micro-level is counterproductive due to lesser conformability. As a result, protuberance obstructs mucosa from entering the miniature chamber of the sucker and inhibits the creation of a negative pressure (Figure 3A; Figure S9a, Supporting Information).<sup>[37]</sup> The described phenomenon becomes more apparent when larger preloads are applied (Figure S9b, Supporting Information). On the other hand, the OS seemed to be more effective than its dimensional counterpart without protuberance, OH 10/15. Higher maximum stress values for the OS group could be either because the protrusion increases the contact with the mucosa, or due to OH 10/15's micro-dimensions that prevented the stiff and firm mucosa of the hard palate from entering the chamber. The larger dimensions and absence of protuberance in OH 50/52 and OH 100/102 led to higher maximum stress, which allowed the mucosa to enter the sucker freely and conform to the shape of the chamber (Figure 3B). We also found increased work of adhesion for non-coated groups with topographies under larger preloads (0.7 N), suggesting that longer displacement prior to complete separation occurs in the presence of topographies.

### 2.5. Quantitative Adhesion Test with Keratin-Coated Topographies

Apart from OH 50/52, keratin-coated groups demonstrated significantly ( $P < 0.0001$ ) improved adhesion than their non-coated counterparts (Figure 2J). Moreover, previously underperformed non-patterned and OS groups showed a twofold increase in maximum stress compared to the non-coated equals across all

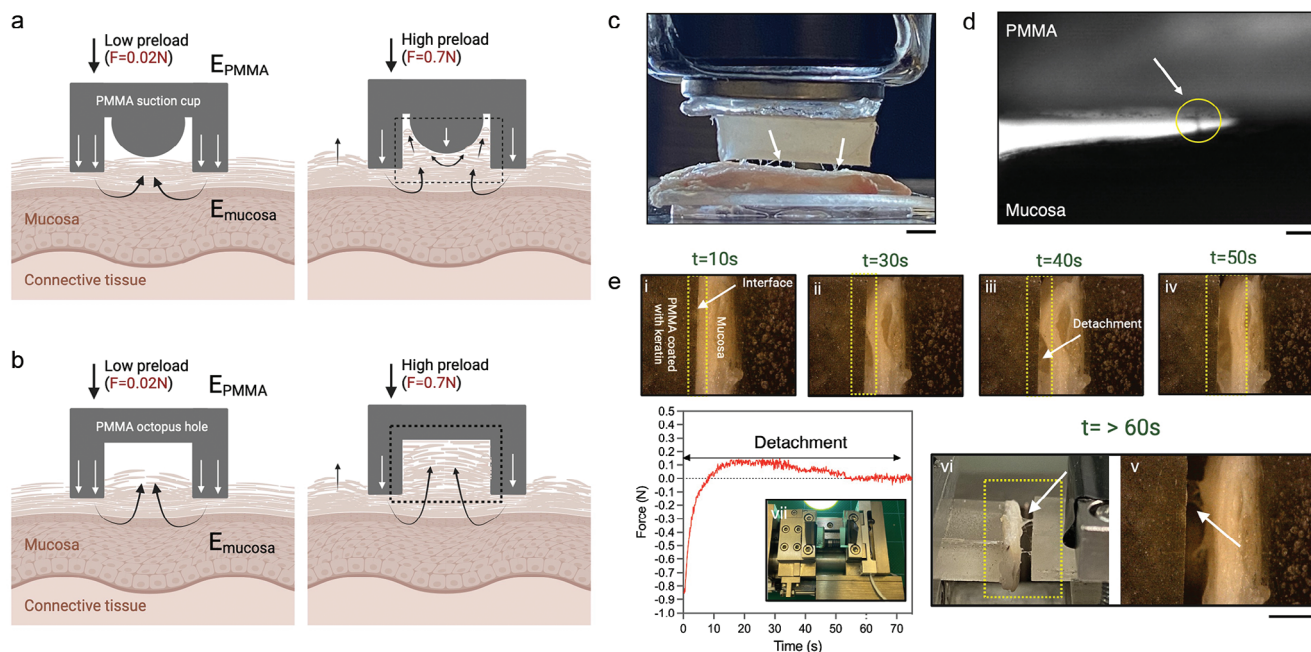


**Figure 3.** Adhesion mechanisms for topographies and keratin. A) Schematic illustration shows detachment mechanism of OS group with protuberance which prevents the penetration of mucosa into the chamber, especially under a large loading (0.7 N). B) Schematic illustration depicts an OH group. The absence of protuberance and large dimensions allow mucosa to be distributed within the chamber, resulting in better mucoadhesion between mucosa and acrylic block ( $E$  = elastic modulus). C) The formation of microstrings (arrows) during detachment is visible by naked eye. Scale bar, 2 mm. D) High-speed camera also demonstrates the presence of microtopographies (arrow) while using large-scale tensile testing machine. Scale bar, 2 mm. E) The stretching of microstrings is observed following the detachment and a deflection on the force-time curve. Scale bar, (i-v) 3 mm.

preloads. Contrary to non-coated samples, the maximum stress of keratin-based topographies increased with the preload size, i.e., the greater the preload, the higher the maximum stress. Only the non-patterned surface remained insensitive to the preload change. Total work of adhesion ( $W_{adh}$ ) proportionally followed this preload-dependent trend with significant increases in samples with topographies. An experiment with the lightweight tensile machine confirmed improved results for the OS and non-patterned samples coated with 5% w/v hair keratin, despite structural differences and variations in amino acid content in comparison to wool keratin (Figure S8b,c, Supporting Information).<sup>[72]</sup> Keratin, on the other hand, did not exhibit higher maximum stress values than the commercial denture adhesive (Figure 2I), which might be attributed to the adhesive's higher viscosity relative to the thin keratin layer.

We correlated the effectiveness of keratin with the available surface area required for keratin deposition, as well as the dimension and density of topographies. Specifically, the actual surface area for keratin deposition decreases for the cumulative surfaces of present topographies. During spin-coating, irregularities imposed by topographical features disrupt the even keratin coating, leading to its accumulations in areas between the topographies (Figure S5, Supporting Information). Conversely, non-patterned groups do not have topographies and therefore enable uniform distribution of keratin. The OS group with the protuberance positioned closer to the surface, compensated the reduced area, and provided a supplementary area for the keratin settlement. Finally, in the OH groups with larger diameters (OH 100/102 and

OH 200/202), the keratin could not bridge the gaps caused by the wide diameters, resulting in its accumulation on the bottom of the topographies. This significantly improved adhesion, especially under higher preloads when the bottom was in contact with the mucosa (Figure 3A). Although the protuberance was previously identified as a potential contributing factor to the reduced adhesion of the non-coated small-scale OS groups, it appears that the protuberance and keratin coating may have synergistic effect.

## 2.6. In Situ Analysis of the Keratin Mediated Adhesion

Previous large-scale and lightweight tensile testing machines showed the formation of microstrings during the retraction of keratin-coated non-patterned groups (Figure 3C,D). Initially, we hypothesized that the strings were responsible for the longer deflection on the force-displacement curve when keratin was present. Therefore, we subjected keratin-coated, non-patterned groups (Figure 3E) to the in situ micro tensile testing with live microscopy. We compared results with the non-coated, non-patterned groups (Figure S10, Supporting Information). Retraction was observed macroscopically and microscopically. The final separation was defined when the mucosa detached from the acrylic surface macroscopically, which resulted in a deflection on the force-time curve (Figure 3E). Upon deflection, further separation between the acrylic and mucosa was followed by the formation of microstrings arising from the superficial

layers of mucosa. Light microscopy confirmed the presence of microstrings, stretching from 0.5 mm to 1 mm in length at the failure (Movie S3, Supporting Information). Conversely, the microstrings were not visible on the surface of the mucosa after its contact with the non-coated acrylic sample (Figure S10c,d, and Movie S4, Supporting Information). Nevertheless, microstrings did not cause additional fluctuations in the force-time curve as we initially hypothesized.

## 2.7. Influence of Different Keratin Concentrations and Batch Variability on Adhesion Performance

We tested how different keratin concentrations would affect the mucoadhesion on non-patterned groups, specifically 7.5% w/v and 10% w/v. The results indicated that the preload dependence persisted, aligning with our earlier findings (Figure S11a, Supporting Information). The maximum detachment forces were notably higher for our optimal concentration of 5% w/v keratin across all preloads. It is noteworthy that the maximum detachment force for 10% w/v significantly increased when 0.7 N preload was applied, reaching a similar range of detachment forces as the 5% w/v concentration. The total work of adhesion was greater for higher keratin concentrations when preloads of 0.3 N and above were applied, with 10% w/v attaining the highest results (Figure S11b, Supporting Information). Keratin-mediated adhesion is enhanced with greater preloads and higher % w/v concentrations. The relationship between keratin, preload, and concentration may be crucial for activating interactions with the keratinized mucosa. The reproducibility of keratin's adhesiveness to mucosa was demonstrated across different batches, with results available in the Supporting Information (Figure S11c,d, Supporting Information).

## 2.8. Degradation of Keratin Coating

Due to keratin's high cysteine content,<sup>[47]</sup> we measured the concentration of free sulfhydryl (-SH) groups produced as a result of cysteine degradation. Our data suggest that the concentration of -SH groups remained low for all tested groups (distilled water, artificial saliva, human saliva) and controls (control distilled water, control artificial saliva) within the first 3 h, while higher concentrations were observed in the control group containing human saliva. The test group with keratin-coated PMMA in human saliva peaked on day 1, similar to the peak observed in the control human saliva group, although the latter showed a twofold higher concentration (Figure S12a,b, Supporting Information). Moreover, the control human saliva demonstrated higher -SH concentrations throughout the experiment, which aligns with the natural presence of thiols in saliva.<sup>[73,74]</sup> By day 7, both the control and test human saliva samples reached similar -SH concentrations. These findings suggest that keratin did not alter the sulfhydryl content of the saliva, demonstrating its ability to withstand various conditions and environments, including the proteolytic activity of salivary enzymes.<sup>[47]</sup> Additionally, the keratin coating on PMMA blocks remained visible under SEM 10 d after the incubation in all tested environments (Figure S12c, Supporting Information).

## 2.9. Optimization of the Ex Vivo Setup

To derive optimal results from ex vivo tests, it was essential to replicate the oral environment precisely. Toward this goal, we compared the stiffness of mucosa with light body polyvinyl siloxane gingival mask, often used as a mimic for gingival tissues in dentistry,<sup>[75]</sup> and the range of denture materials with different compliances. Gingival mask exhibited Young's modulus of  $E = 1.31 \pm 0.33$  MPa making it the closest counterpart to the Young's modulus of keratinized mucosa, which is  $E = 7.25 \pm 2.18$  MPa (Figure S13a,c and Table S1, Supporting Information). We also introduced a PDMS-PEG block copolymer-BCP,<sup>[76]</sup> aiming to acquire comparable wettability of gingival mask to the mucosa. This adjustment resulted in a significant reduction in the final contact angle value from  $\theta = 107.3 \pm 2.13^\circ$  to  $\theta = 43.5 \pm 9.97^\circ$  (Figure S13d,e, Supporting Information). Subsequently, gingival mask was coated with keratin to mimic keratinized layer of mucosa whenever indicated for the keratin-mediated (moist) environment. Approximately 50% of the gingival mask's surface was covered with distilled water to mimic mucosa's natural hydration.

## 2.10. Ex Vivo Denture Adhesion Test

The architecture of a natural suction cup was replicated digitally and merged with a digital file of a conventional denture in 3D CAM software (Figure 4A,B). After, suction cups were multiplied and placed onto the fitting surface of a denture in an ordered manner (Figure 4C; Figure S14a–g, Supporting Information). Based on the exposure of octopi suckers, we obtained two types of dentures. One denture type contained embedded suction cups (SC) (Figure 4D) while the other had extruded suction cups (SC-EX) (Figure 4E). We used smooth denture without suction cups as a control. These denture types were further grouped based on the material, as follows: the first group comprised dentures (SC, SC-EX, and smooth) in resin material; the second group consisted of dentures (SC, SC-EX, and smooth) with fitting surfaces fabricated from the soft denture material; and the third group involved resin dentures coated with keratin (SC, SC-EX, and smooth). Dentures with soft material were employed to assess the impact and extent to which the choice of material influences the performance of topographies.

During the adhesion test (Figure 4F), at an average seating force of 17 N, which is a typical force applied by patients during denture placement,<sup>[77]</sup> we found that the SC resin dentures in dry and wet environments showed significantly ( $P < 0.0001$ ) improved adhesion than the denture adhesive (Figure 4G). Moreover, SC resin dentures required significantly higher maximum detachment force (dry:  $2.28 \pm 0.045$  N; wet:  $2 \pm 0.0$  N; saliva:  $1.66 \pm 0.06$  N) than the control resin dentures across all environments (dry:  $1.96 \pm 0.03$  N; wet:  $0.41 \pm 0.07$  N; saliva:  $0.67 \pm 0.01$  N). On the other hand, the SC-EX revealed notably ( $P < 0.0001$ ) improved retention in saliva ( $2.3 \pm 0.2$  N) compared to the SC resin denture ( $1.66 \pm 0.06$  N). Interestingly, the SC resin denture outperformed all dentures with topographies in soft material, which is contrary to the strong adhesion of natural soft suction cups and suggests that at least one rigid substrate is necessary to generate a pressure differential (Figure S15, Supporting Information).<sup>[78]</sup>

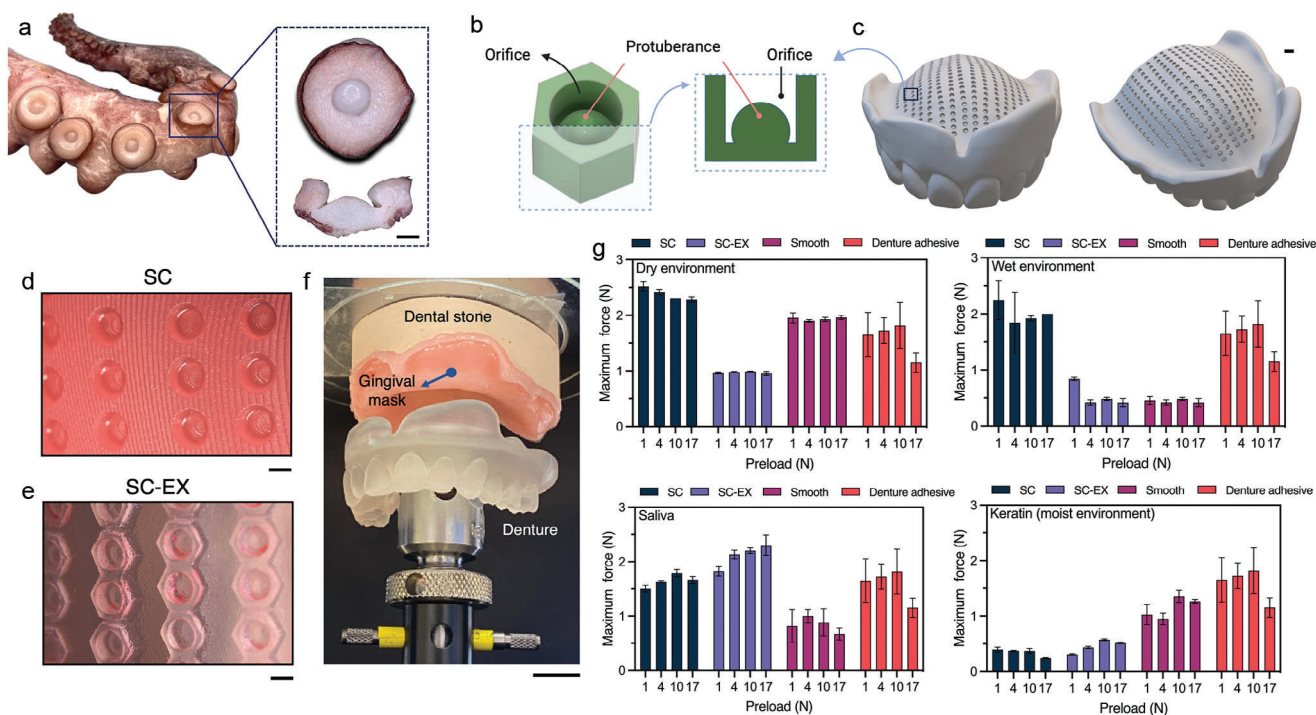


**Figure 4.** Proof of concept application of octopus-like topographies in dentistry. A) *Octopus vulgaris* tentacle with insets representing top-down and cross-sectional projection of an OS. Scale bar, 2 mm. B) STL file of an octopus suction cup model resembling the architecture of a natural suction cup and comprising the orifice and dome-shaped structure – protuberance. C) STL file of dentures with multiple suction cups on a fitting surface. Scale bar, 1 mm. D) The fitting surface of an embedded suction cup denture. Scale bar, 1.5 mm. E) Fitting surface of a denture with extruded suction cups. Scale bar, 1.5 mm. F) The setup for unidirectional pull-off adhesion test, where the denture is detaching from gingival mask (“mucosa”) located on the dental stone model (“hard palate”). Scale bar, 2 cm. G) Profiles of maximum detachment forces for resin dentures across all tested environments. Error bars in the graphs represent standard deviations for the tested groups ( $N = 20$ ). Detailed statistical analysis and multiple comparisons were performed using a two-way ANOVA with a Tukey’s post-test and are summarized in the Supporting Information Tables S1–S5 (Supporting Information).

Preload had minimal impact on the force values across tested dentures. In contrast to the microtopographies, it is plausible that larger suction cups in hard materials offer more space in the orifice for the generation of a negative pressure, which resulted in the improved retention. Keratin significantly ( $P < 0.0001$ ) increased the retention of the keratin-coated control denture ( $1.27 \pm 0.035$  N) than the non-coated control dentures in a wet and salivary-based environment ( $0.48 \pm 0.07$  N), suggesting its potential in the mucoadhesion of biomaterials.

We also compared the total work of adhesion, since it is more determinant for larger surfaces.<sup>[79]</sup> Our findings confirmed the significantly ( $P < 0.0001$ ) improved total work of adhesion for SC resin dentures in dry and wet conditions, especially under the typical denture seating force (preload = 17 N) (Figure S16, Supporting Information). Keratin-coated control dentures showed increased total work of adhesion and preload dependency in comparison to keratin-coated SC and SC-EX dentures in moist environment. The declining adhesion of coated SC and SC-EX dentures reaffirms the surface-dependence of keratin-based systems, i.e., greater surface required for keratin deposition is found on dentures without topographies. Alternatively, keratin might have obliterated the topographies and potentially hindered their effect.

### 3. Conclusion

Over the past two decades, bioinspired adhesion has found its purpose in robotics, drug delivery, wound dressings, and wearable medical devices. To the best of our knowledge, this direction in biomimetics has not been exploited in the dental field to develop bioinspired retentive surfaces. Toward this goal, we investigated octopus-inspired surface topographies and biopolymer keratin as new retention models on the quest for the next generation of complete dentures. The dentures, inspired by octopus design, yielded promising results. However, it is essential to expand the testing beyond laboratory conditions, include more dentures, and evaluate denture’s performance in the dynamic oral environment, including the interaction with natural mucosa.

At present, using two-photon polymerization and direct laser writing to develop micro-suction cups directly on dentures is technically challenging, but the technology is rapidly advancing. Due to the growing needs in industry and engineering, the two-photon polymerization, predominantly utilized in micro- and nanofabrication, can now be used to fabricate objects with dimensions up to several millimeters on large and curved surfaces.<sup>[54,80]</sup> Additionally, advancements in commercial 3D printing, printer resolution, and materials could bring bioinspired dentures closer

to the growing number of edentulous patients, especially the least advantaged and vulnerable ones, who will continue to seek dentures as treatment options for missing teeth. Also, the bioinspired approach could make dentures more sustainable, both financially and environmentally, by replacing synthetic denture adhesives with biopolymers such as keratin. Keratin is a safer and inexpensive alternative that resists degradation under physiological conditions and is not easily broken down by common enzymes found in saliva.<sup>[47]</sup> Keratin's *in vivo* breakdown can be controlled by changing material properties, such as crosslinking density or oxidative properties, yet without the formation of toxic peptide byproducts.<sup>[49]</sup> Because of the absence of genetic material, it does not trigger adverse immune reactions, which makes keratin an ideal cosmetic industry ingredient widely used for hair and skin treatments.<sup>[81]</sup> No evidence has been found in the literature regarding the transmission of diseases associated with keratin derived from xenogeneic epidermal appendageal structures. However, if there are concerns about potential contamination, these can be effectively addressed using gamma radiation to safely sterilize keratin and ensure its suitability for dental applications.<sup>[82,83]</sup>

Ultimately, the application of octopi suckers and keratin might extend beyond dentistry and provide a leap step forward in self-adhesive solutions for moist environments. This could enhance the functionality of hard contact and intraocular lenses, medical or facial prostheses, drug delivery systems, oral patches, and wearable devices.

## 4. Experimental Section

**Fabrication of Si Wafers for PDMS Casting:** Octopus-inspired topographical designs were created with KLayout software (KLayout, Munich, Germany). Two variations of octopus suckers were used – a complex design with a protuberance – OS (Figure 1C,D), and a simplified design, referred to as OH (Figure 1C). OS topographies were printed via two-photon polymerization (Nanoscribe PPGT, 25x objective; NanoFAB, University of Alberta, Edmonton, Canada) in IP-S Nanoscribe resin on a 10 mm × 10 mm patterned area and inside a 25 mm × 25 mm Si chip. The resulting OS design featured components with a 15 μm diameter, 20 μm pitch size, and 15 μm height. A protuberance had a diameter of 12 μm and a height of 9.6 μm, thereby mimicking the protuberance's natural exposure of 80% within the chamber (Figure 1D).<sup>[84]</sup>

OHs were obtained from Si wafers (P-type 100, 10 –20Ω • cm, 150 mm diameter, 675 mm thick; NanoFAB, University of Alberta, Edmonton, Canada) that were previously coated with photoresist (AZ 1529, thickness = 3.5 μm). Afterward, OH patterns were created by exposing the photoresist to light (direct write laser lithography) and removing it from the regions that will be etched. As a result, densely populated OH designs with various diameter/pitch sizes (Figure 1C) were laid out within 24 cells (dimensions 15.7 mm × 27.1 mm) on the wafer inside a 5 mm edge exclusion area. For adhesion tests, four OH microstructures were opted for: OH 10/15, OH 50/52, OH 100/102, and OH 200/202. These microstructures had varying diameters of 10 μm, 50 μm, 100 μm, and 200 μm alongside the pitch sizes of 15 μm, 52 μm, 102 μm, and 202 μm, respectively (Figure 1C). The depth of all OH microstructures was standardized at 15 μm. All Si wafers were mantled with a parylene-C coating (Para Tech Coating UK Ltd, Northampton, UK), resulting in a layer thickness of 0.5 μm ± 10%.

**Fabrication of Negative Poly(dimethylsiloxane) Molds:** Poly(dimethylsiloxane) (PDMS) (Sylgard 184 Dow Corning Co; Midland, MI, USA) was mixed in a recommended 10:1 ratio and distributed on a Si wafer to achieve a layer thickness of ≈5 mm. This thickness was sufficient to prevent the lifting and bending of PDMS in the next step

during acrylic polymerization. Si wafers with PDMS were left in the oven at 100 °C for 75 min (Figure S1, Supporting Information).

**Preparation of Positive Acrylic Blocks with Topographies:** PDMS sheet with topographies faced upward was placed at the base of a silicone mold (Figure S3a, Supporting Information). Subsequently, self-cured PMMA (Oracryl, Bracon, Heathfield, UK) mixed in a ratio of 3:1, was poured into rubber molds and covered with a metal piece to ensure better replication. After 24 h, acrylic blocks measuring 10 mm × 10 mm × 3 mm were released from the molds and sharp edges were smoothed. Additionally, we created a control group of non-patterned acrylic blocks was created.

**Microscopic Examination of Samples:** The Keyence VHX-7000 4K digital microscope (Keyence, Osaka, Japan) was used to inspect Si wafers and the replication success of negative PDMS molds. Acrylic blocks were examined with the high-resolution JEOL JSM 7800F Prime SEM (JEOL UK Ltd, Welwyn Garden City, UK). Prior to SEM analysis, an 8 nm thick conductive gold coating was deposited on the specimens to enhance imaging quality.

**Keratin Extraction:** Extraction was performed as reported in the literature with minor adjustments.<sup>[47]</sup> Sheep's wool (10 g) was obtained from the local farm, washed in distilled water, and left to dry overnight. Successively, Soxhlet extraction was performed. Briefly, 150 mL of hexane (Hexane for HPLC, ≥97%, Sigma Aldrich, Dorset, UK) and 150 mL of dichloromethane (Dichloromethane, ≥99.8%, Fisher Scientific, Loughborough, UK) (ratio 1:1) were mixed in a rounded flask at 65 °C for 6 h. The following day, delipidated wool was combined with 180 mL 7 M urea (Urea powder, ≥98%, Sigma Aldrich, Dorset, UK), 6 g of SDS (SDS, ≥99%, Sigma Aldrich, Dorset, UK), and 15 mL of mercaptoethanol (2-Mercaptoethanol, ≥99%, Sigma Aldrich, Dorset, UK), allowing the mixture to stir overnight at 50 °C. Wool was removed from the flask, and the remaining content was centrifuged for 25 min at the speed of 6000 rpm and a temperature of 4 °C (Sorvall Lynx 6000, Fisher Scientific, Loughborough, UK). The supernatant was transferred to the dialysis membranes (14 kDa) and the dialysis was conducted over 3–4 d with periodic water renewal. Finally, the purified keratin solution was freeze-dried over the next 5 d.

**Keratin Coating of Acrylic Blocks:** Lyophilized keratin powder was dissolved in ultrapure water previously adjusted to pH 7.2 to prepare solutions at concentrations of 5% w/v, 7.5% w/v, and 10% w/v. A vortex mixer (Fisher Scientific, Loughborough, UK) was used at 25 × 100 rpm at room temperature until the solution became clear. Next, 100 μL of keratin solution was applied to the center of the static acrylic block on a spin coater (Instras Scientific, SCK-300P; New Jersey, NY, USA). The acrylic block started rapidly accelerating until reaching the high-speed velocity of 3000 rpm for 30 s (Figure S4a, Supporting Information). All coated acrylic blocks were left at room temperature to dry for 15 min.

**Surface Characterization:** ImageJ software (National Institutes of Health, Bethesda, Maryland, USA) was used to measure the thickness of cross-sections of keratin coatings on images taken with the high-resolution JEOL JSM 7800F Prime SEM (JEOL UK Ltd, Welwyn Garden City, UK).

AFM was employed to assess the state of keratin before and after assembly by examining changes in surface roughness. Keratin was dissolved in ultrapure water and placed on a glass slide. The sample was scanned in tapping mode using Nanoscope III Multimode AFM controller (Digital Instruments, California, USA) and cantilever OTESPA-R3 (Bruker, California, USA). Images were flattened to remove curvature and slope before the interpretation with NanoScope analysis software (Bruker, California, USA).

The wettability of acrylic blocks with and without the keratin layer was evaluated through the contact angle measurement. Logitech C920 HD 1080p Pro Camera (Logitech, Lausanne, Switzerland) was used and measurements were performed at room temperature (23 °C) and relative humidity (≈35%). 50 μL of distilled water was released onto an acrylic's surface and the pictures were captured within the predetermined interval: 1 min, 10 min, 20 min, 40 min, and 1 h. Contact angle measurements were performed with ImageJ software (National Institutes of Health, Bethesda, Maryland, USA).

SDS (Sodium dodecyl sulfate,  $\geq 99\%$ , Sigma Aldrich, Dorset, UK) was dissolved in distilled water to its solubility limit ( $150 \text{ g L}^{-1}$ ) at room temperature. The contact angle values of water droplets were measured on the keratin-coated acrylic surface, and they were compared to those of SDS droplets.

**Degradation of Keratin Coating:** Ellman's assay was used to quantify the sulfhydryl groups based on the molar extinction coefficient of 2-nitro-5-thiobenzoic acid (TNB). In the assay, Ellman's reagent (ThermoFisher Scientific, Loughborough, UK) is 5,5'-dithio-bis-(2-nitrobenzoic acid) (DTNB) that reacts with sulfhydryl (-SH) groups and produces a yellow-colored TNB anion.<sup>[85]</sup> To assess keratin coating degradation, PMMA blocks with 5% w/v keratin were placed in tubes containing 5 mL of different solutions: distilled water, artificial saliva, and unstimulated human saliva. Human saliva collection was approved by the King's College London Ethics Committee (approval number RESCM-22/23-34267, courtesy of Prof. Guy Carpenter). The blocks were incubated at 37 °C, and samples were taken at predetermined time points including 30 min, 90 min, 3 h, 17 h, 1 d, 3 d, and 7 d. Another set of solutions without PMMA blocks served as negative controls and blanks. For each sample, 250  $\mu\text{L}$  of the tested solution was mixed with 50  $\mu\text{L}$  of Ellman's reagent and 2.5 mL of reaction buffer (0.1 M sodium phosphate, pH 8.0, 1 mM EDTA). The mixtures were incubated at room temperature for 15 min, and absorbance was measured in triplicates at 412 nm using a NanoDrop 1000 UV/VIS Spectrophotometer (ThermoFisher Scientific, Loughborough, UK). After 10 days of incubation, PMMA blocks with keratin were observed under SEM to confirm the presence of keratin coating.

**Mechanical Testing – Qualitative Pull-Off Adhesion Test:** Preliminary adhesion tests were carried out in moist and wet environments (distilled water), and the two flat acrylic blocks were compared, with and without the keratin. Full-thickness sheep's oral keratinized mucosa was obtained from the slaughterhouse, cut into size  $3 \text{ cm} \times 1.5 \text{ cm}$ , and glued to the solid surface. Coated and non-coated acrylic blocks were manually pressed onto a mucosa's explant and pulled off (Movies S1 and S2, Supporting Information).

**Mechanical Testing – Quantitative Pull-Off Adhesion Test:** Uniaxial pull-off test mode on the Instron machine 5569A series (Instron, High Wycombe, UK) was employed and acrylic blocks (A) were successively mounted to the moving crosshead. The lower frame was fixed and used as a pedestal for the mucosa (M) (Figure 2G). All blocks were submitted to different preloads (0.02 N, 0.3 N, 0.5 N, and 0.7 N using a load cell of 10 N. Each preload was applied five times ( $N = 20$  repeats per group) and held for 20 s. After, the loading cell started retraction at a speed of  $1 \text{ mm min}^{-1}$ . As a positive control, 40 mg of denture adhesive cream (Fixodent, Procter and Gamble, Weybridge, UK) was used. The graphs that depicted the force were plotted as a function of displacement for each preload, and the maximum force ( $F_{\text{max}}$ ), normal maximum (adhesion) stress ( $\sigma_{\text{max}}$ ), and the total work of adhesion (area under the curve) ( $W_{\text{adh}}$ ) (Figure 2H) were analyzed. The maximum (adhesion) stress was determined as follows:

$$\sigma_{\text{max}} = \frac{F_{\text{max}}}{A} \quad (1)$$

where  $\sigma_{\text{max}}$  is the maximum (adhesion) stress,  $F_{\text{max}}$  is the maximum detachment force that the interface can endure before breaking, and  $A$  represents the total area of the interface. The magnitude of the maximum detachment force and the adhesion stress was contingent on the strength of the most vulnerable element within the joint, either physical or chemical source of adhesion.<sup>[86]</sup> The total work of adhesion ( $W_{\text{adh}}$ ) corresponds to the area beneath the force-displacement curve.<sup>[87–89]</sup> Due to the complexity of interactions between soft mucosa and hard acrylic, as well as the incompatibility of their Young's moduli, the potential energy dissipation that occurs at the interface of a contact had to be considered. Therefore, the displacement was corrected as described:

$$x' = x - \left[ \left( \frac{h_1 * \sigma_{\text{max}}}{E_1} \right) - \left( \frac{h_2 * \sigma_{\text{max}}}{E_2} \right) \right] \quad (2)$$

where  $x'$  is the corrected displacement;  $x$  is the initial displacement;  $\sigma_{\text{max}}$  is the maximum stress;  $h_1$  is height of the acrylic;  $E_1$  is the Young's modulus of the acrylic;  $h_2$  is the height of mucosa explant; and  $E_2$  is the Young's modulus of the mucosa. The corrected  $x'$  value was afterward considered as a new displacement, based on which the definitive total work of adhesion was estimated.

Additionally, a pull-off uniaxial test was performed with the lightweight tensile tester (ForceBoard, Industrial Dynamics Sweden AB, Järfälla, Sweden). The fixed stage of the machine held the mucosa explant while the acrylic blocks were coupled with the moving jig (Figure S8a, Supporting Information). Acrylic blocks that were morphologically and dimensionally identical to blocks from the Instron experiment were used. However, parameters were changed relative to the Instron setup. Hair keratin (5% w/v), higher speed ( $0.02 \text{ mm s}^{-1}$ ), 20 N load cell, and preloads of 0.1 N, 0.3 N, 0.5 N, and 0.7 N were used. A high-speed camera was obtained to provide a macroscopical overview of the interface between the acrylic and the mucosa (frame rate: 125 pfs; shutter speed = 1/frame s; resolution =  $640 \times 480$ ).

To understand the events occurring at the interface between acrylic and mucosa, a micro tensile test and live imaging were performed. A new sets of acrylic blocks measuring  $15 \text{ mm} \times 11 \text{ mm} \times 4 \text{ mm}$  that were polished with grinding foils #P800, #P1000, #P2000, successively, were fabricated. The opposite ends of acrylic blocks were clamped by the grip of the microtester (300 N tensile stage) (Deben, Bury St Edmunds, UK) (Figure S10a, Supporting Information) while the cross-section surfaces in the middle of the gauge (surface area =  $44 \text{ mm}^2$ ) were observed under the stereo microscope (Olympus SZ61, Shinjuku, Japan). The mucosa was glued onto a polished surface of one block and brought in contact with the surface of the adjacent block (Figure 3E and Figure S10b, Supporting Information). Blocks were kept in contact for  $\approx 20 \text{ s}$  at the preload of 1 N. The retraction started in opposite directions at the constant rate of  $1 \text{ mm min}^{-1}$  (Movies S3 and S4, Supporting Information).

All dentures were subjected to uniaxial pull-off adhesion test (Instron machine 5569A series, load cell 500 N, crosshead speed  $1 \text{ mm min}^{-1}$ ,  $N = 20$ ) under various conditions (dry, distilled water, artificial saliva, keratin-based/moist environment) and varying preloads (1 N, 4 N, 10 N, 17 N) (Figure 4F). Gingival mask (Gingifast, Zhermack, Badia Polesine, Italy) was used as a proxy for mucosa which underwent modification with PDMS-PEG block copolymer (BCP) (Gelest, product code DBE-712, Morrisville, PA, USA) to enhance its wetting properties.<sup>[58,74]</sup> Afterward, modified gingival mask was applied on the surface of a dental stone that served as a replacement for the hard palate.

For the experiment with keratin-coated dentures, the 5% w/v keratin solution was sprayed on the hydrophilic gingival mask to mimic the keratinized mucosa and achieve moist environment.

**Tensile Test:** Hard PMMA (Oracryl, Bracon, Heathfield, UK) and commercial dental materials, Coe-Soft and GC reline (GC America Inc. Alsip, IL, USA), Molloplast B (Detax GmbH, Ettlingen, Germany), and Gingifast (Zhermack, Badia Polesine, Italy) were selected for the tensile test to compare their Young's moduli to the sheep's keratinized mucosa. The 3 mm thick and 75 mm long dumbbell-shaped samples ( $N = 3$ ) were obtained for each of the abovementioned materials (Figure S13a, Supporting Information). The dumbbell's neck was 26 mm long and 5 mm wide (Figure S13b, Supporting Information). Samples were subjected to uniaxial tensile test mode on the Instron machine (5569A series) and stretched at the constant speed of  $20 \text{ mm min}^{-1}$  until the break. Afterward, the final stress-strain curve was plotted, and the Young's moduli (Figure S13c, Supporting Information) was estimated.

**Denture Design and DLP 3D Printing:** The main small-scale OS group was converted to digital stereolithography, ".stl" format (Figure 4B). First, the OS topographies were printed individually at various sizes to assess the resolution (Figure S14a, Supporting Information). The final design was configured to account for this, and the size of each sucker diameter was 1.7 mm and sucker height 1.5 mm. Using the Fusion Autodesk 360 (Adobe, San Jose, CA, USA), digital files of an upper non-patterned denture (Figure S14b-e, Supporting Information) and OS model were combined to generate dentures featuring embedded (SC) and extruded (SC-EX) topographies (Figure 4D,E). Additionally, a non-patterned denture was printed to serve

as a control. Dentures were printed in resin (Denture Base EU SprintRay, Weiterstadt, Germany) using SprintRay Pro S55 DLP 3D printer (Sprintray, Los Angeles, CA, USA/Weiterstadt, Germany) with a layer thickness of 100  $\mu\text{m}$ . Post-printing, the dentures were washed in isopropyl alcohol (Propan-2-ol,  $\geq 99.8\%$ , ThermoFisher Scientific, Loughborough, UK) for 10 min and placed under ultraviolet light (ProCure-2, Weiterstadt, Germany) for 5 min to complete the curing (Figure S14f,g, Supporting Information). Following the same procedure, another set of resin dentures (SC, SC-EX, and non-patterned control) were created, and they were coated with keratin upon their fabrication. The method adhered to the previously described spin-coating procedure (5% w/v, 1500 rpm – 30 s) (Figure S17, Supporting Information).

**Fabrication of Dentures with Topographies in Soft Material:** Dentures with soft material were employed as an additional group. Before relining the denture: 1) a hard cast negative of the topographies was generated to withstand the reline flasking and packing process, and 2) the denture was relined with cold cure acrylic to allow support and adherence for relining material (Figure S18, Supporting Information). To create the substrate master cast with a negative topography surface, the impression of the denture with topographies was taken with a silicone. This negative silicone model was scanned, and a resin maxillary cast was printed (Figure S18a, Supporting Information). The fitting surface of the non-patterned denture was reduced completely while the dental arch with provisional teeth was preserved (Figure S18b, Supporting Information). This was to allow space for acrylic ( $\approx 1$  mm) and relining material ( $\approx 1$  mm). Afterward, the  $\approx 2$  mm void was filled with two layers of pink wax, and the provisional dental arch was seated on the top. Resin cast and wax layers were invested in a sectional flask to form the denture base. After the plaster had completely set, the wax was boiled out for 5 min. Cold-cured PMMA (Diamond D acrylic, Keystone Industries, Singen, Germany) was mixed up and placed over the dental ridge, and the plaster was coated with an isolator (Unifol, Perident Dental Products, Vallina, Italy) to prevent the PMMA from attaching to the cast (Figure S18c, Supporting Information). The surface of the PMMA was again reduced slightly, and relining material was placed over the pre-pressed PMMA denture base. The negative cast was covered with a separating agent (3D Isoliermittel, Dentaurum, Ispringen, Germany) (Figure S18d) to prevent the relining material from sticking (Figure S18e, Supporting Information). The flask was pressed at 100 kPa at set interval, then opened to remove excess material, and pressed again for an additional 15 min at 100 kPa. To complete polymerization, the flask was left in cold water that was slowly heated to 74  $^{\circ}\text{C}$  for 8 h, then cooled slowly to room temperature overnight (Figure S18f, Supporting Information).

**Statistical Analysis:** Data pre-processing and cleaning were conducted using GraphPad (Prism, La Jolla, USA) and the pandas library in Python. The normality of the data distribution was assessed with the Shapiro-Wilk test. Where data did not meet the assumption of normality (i.e., batch-to-batch variability,  $N = 15$ ), the Kruskal-Wallis test was employed, followed by Dunn's post-hoc test. Statistics for the pull-off adhesion test was conducted using a two-way analysis of variance (ANOVA) followed by post hoc Tukey's and/or Šidák's tests (GraphPad, Prism, La Jolla, USA) with  $N = 20$  repeats per selected group. The strength and the significance level were arranged at  $P \leq 0.05$  and 95% confidence interval. Wherever indicated, quantitative data were plotted as the mean  $\pm$  standard deviation (SD), with error bars representing the standard deviation.

## Supporting Information

Supporting Information is available from the Wiley Online Library or from the author.

## Acknowledgements

Conceptualization was by S.E., E.D., and O.A.; Methodology was performed by E.D., S.E., and O.A.; Formal analysis was carried out by E.D.; Investigation was conducted by E.D., L.C., N.K., N.A., S.W., S.G., Y.L., N.R., P.B., K.C., and E.W.; Visualization was carried out by E.D.; Supervision was

by S.E., O.A., N.M.P., S.W., F.G., and Z.J.Z.; Original draft was by E.D.; Review & editing was by S.E., O.A., Z.J.Z., S.W., and E.D. The authors thank M. Baseeruddin for assisting with denture design; Prof. G. Carpenter and S. Huang (King's College London) for providing the ethical approval for the collection of human saliva; and Prof. K. Carneiro and Dr. D. Athanasidou (University of Toronto) for the assistance with the AFM. The authors thank P. Pilecki and Dr. D. White (Centre for Oral, Clinical & Translational Sciences) and the Centre for Ultrastructural Imaging (CUI) at King's College London for the technical support services. Part of this work was conducted at the University of Alberta nanoFAB center. The authors would like to acknowledge the funding from King's PGR International Studentship, National Institute of Health Research UK, and the Academy of Medical Sciences.

## Conflict of Interest

The authors declare no conflict of interest.

## Data Availability Statement

The data that support the findings of this study are available from the corresponding author upon reasonable request.

## Keywords

3D printing, biomimetics, complete dentures, keratin, octopus, pull-off force, retention

Received: June 11, 2024

Revised: October 31, 2024

Published online: November 19, 2024

- [1] N. Kassebaum, E. Bernabé, M. Dahiya, B. Bhandari, C. Murray, W. Marcenes, *J. Dent. Res.* **2014**, *93*, 20S.
- [2] V. Baelum, W. Van Palenstein Helderma, A. Hugoson, R. Yee, O. Fejerskov, *J. Oral Rehabil.* **2007**, *34*, 872.
- [3] A. Kailembo, R. Preet, J. S. Williams, *BMC Oral Health* **2017**, *17*, 1.
- [4] T. Vos, S. S. Lim, C. Abbafati, K. M. Abbas, M. Abbasi, M. Abbasifard, M. Abbasi-Kangevari, H. Abbastabar, F. Abd-Allah, A. Abdelalim, *Lancet* **2020**, *396*, 1204.
- [5] M. A. Peres, L. M. Macpherson, R. J. Weyant, B. Daly, R. Venturelli, M. R. Mathur, S. Listl, R. K. Celeste, C. C. Guarnizo-Herreño, C. Kearns, *Lancet* **2019**, *394*, 249.
- [6] Global oral health status report: Towards universal health coverage for oral health by 2030, **2022**, <https://www.who.int/publications/i/item/9789240061484> (accessed: February 2024).
- [7] R. Borg-Bartolo, A. Rocuzzo, P. Molinero-Mourelle, M. Schimmel, K. Gambetta-Tessini, A. Chaurasia, R. Koca-Ünsal, C. Tennert, R. Giacaman, G. Campus, *J. Dent.* **2022**, *127*, 104335.
- [8] S. Tyrovolas, A. Koyanagi, D. B. Panagiotakos, J. M. Haro, N. J. Kassebaum, V. Chrepa, G. A. Kotsakis, *Sci. Rep.* **2016**, *6*, 37083.
- [9] J. Patel, J. Wallace, M. Doshi, M. Gadanya, I. B. Yahya, J. Roseman, P. Srisilapanan, *Lancet Healthy Longev.* **2021**, *2*, E521.
- [10] H. Olofsson, E. L. Ulander, Y. Gustafson, C. Hörnsten, *Scand. J. Public Health* **2018**, *46*, 690.
- [11] B. Darvell, R. Clark, *Br. Dent. J.* **2000**, *189*, 248.
- [12] M. D. Murray, B. W. Darvell, *Aust. Dent. J.* **1993**, *38*, 216.
- [13] J. Ko, K. Cho, S. W. Han, H. K. Sung, S. W. Baek, W.-G. Koh, J. S. Yoon, *Colloids Surf. B* **2017**, *158*, 287.
- [14] A. K. Riau, D. Mondal, G. H. Yam, M. Setiawan, B. Liedberg, S. S. Venkatraman, J. S. Mehta, *ACS Appl. Mater. Interfaces* **2015**, *7*, 21690.

- [15] B. B. Chamberlain, M. E. Razzoog, E. Robinson, *J. Prosthet. Dent.* **1984**, *52*, 744.
- [16] Z. Al-Dwairi, E. Lynch, *Gerodontology* **2014**, *31*, 49.
- [17] N. Ikemura, Y. Sato, J. Furuya, O. Shimodaira, K. Takeda, T. Kakuta, K. Yamane, N. Kitagawa, *BMC Oral Health* **2021**, *21*, 1.
- [18] D. R. Kore, M. T. Kattadiyil, D. B. Hall, K. Bahjri, *J. Prosthet. Dent.* **2013**, *110*, 488.
- [19] F. Zhang, Y. An, N. Roohpour, A. H. Barber, J. Gautrot, *Dent. Mater.* **2018**, *34*, 10.
- [20] N. S. Ereifej, Y. G. Oweis, M. Abu-Awwad, *BMC Oral Health* **2023**, *23*, 1.
- [21] D. R. Burns, *J. Prosthodont.* **2000**, *9*, 37.
- [22] J. Feine, *Int. J. Prosthodont.* **2002**, *15*, 413.
- [23] L. F. Cooper, *Periodontol* **2000**, *2000*, 103.
- [24] S. Otto, C. Schreyer, S. Hafner, G. Mast, M. Ehrenfeld, S. Stürzenbaum, C. Pautke, *J. Craniomaxillofac. Surg.* **2012**, *40*, 303.
- [25] K. C. Yerit, M. Posch, M. Seemann, S. Hainich, O. Dörtbudak, D. Turhani, H. Özyuvaci, F. Watzinger, R. Ewers, *Clin. Oral Implants Res.* **2006**, *17*, 337.
- [26] C. Scully, C. Madrid, J. Bagan, *Implant Dent.* **2006**, *15*, 212.
- [27] C. Scully, J. Hobkirk, P. D. Dios, *J. Oral Rehabil.* **2007**, *34*, 590.
- [28] A. A. Hashem, N. M. Claffey, B. O'Connell, *Int. J. Oral Maxillofac. Implants* **2006**, *21*, 943.
- [29] B. Pommer, W. Zechner, G. Watzak, C. Ulm, G. Watzek, G. Tepper, *Clin. Oral Implants Res.* **2011**, *22*, 106.
- [30] C. W. Douglass, A. Shih, L. Ostry, *J. Prosthet. Dent.* **2002**, *87*, 5.
- [31] M. Kikuchi, F. Ghani, M. Watanabe, *J. Prosthet. Dent.* **1999**, *81*, 399.
- [32] R. Vasant, G. Bassi, *Br. Dent. J.* **2012**, *212*, 431.
- [33] A. C. Jermyn, *J. Prosthet. Dent.* **1967**, *18*, 316.
- [34] M. Ordulu, Y. Emes, M. Ates, I. Aktas, S. Yalcin, *Quintessence Int* **2006**, *37*, 659.
- [35] O. Cayetano, M. E. Boone, *J. Am. Dent. Assoc.* **1987**, *115*, 577.
- [36] B. Bhushan, *Philos. Trans. A. Math. Phys. Eng. Sci.* **2009**, *367*, 1445.
- [37] S. Baik, H. J. Lee, D. W. Kim, H. Min, C. Pang, *ACS Appl. Mater. Interfaces* **2019**, *11*, 25674.
- [38] G. Meloni, O. Tricinci, A. Degl'Innocenti, B. Mazzolai, *Sci. Rep.* **2020**, *10*, 15480.
- [39] H. Lee, D.-S. Um, Y. Lee, S. Lim, H.-j. Kim, H. Ko, *Adv. Mater.* **2016**, *28*, 7457.
- [40] S. Chun, D. W. Kim, S. Baik, H. J. Lee, J. H. Lee, S. H. Bhang, C. Pang, *Adv. Funct. Mater.* **2018**, *28*, 1805224.
- [41] F. Tramacere, M. Follador, N. Pugno, B. Mazzolai, *Bioinspir. Biomim.* **2015**, *10*, 035004.
- [42] S. Baik, D. W. Kim, Y. Park, T.-J. Lee, S. Ho Bhang, C. Pang, *Nature* **2017**, *546*, 396.
- [43] Y. Wu, X. Li, H. Tian, D. Wang, J. Zhang, L. Wang, J. Shao, *Adv. Funct. Mater.* **2023**, *33*, 2210562.
- [44] Z. Luo, D. Klein Cerrejon, S. Römer, N. Zoratto, J.-C. Leroux, *Sci. Transl. Med.* **2023**, *15*, eabq1887.
- [45] S. Baik, H. J. Lee, D. W. Kim, J. W. Kim, Y. Lee, C. Pang, *Adv. Mater.* **2019**, *31*, 1803309.
- [46] B. S. Lazarus, C. Chadha, A. Velasco-Hogan, J. D. Barbosa, I. Jasiuk, M. A. Meyers, *isience* **2021**, *24*, 102798.
- [47] A. Shavandi, T. H. Silva, A. A. Bekhit, A. E.-D. A. Bekhit, *Biomater. Sci.* **2017**, *5*, 1699.
- [48] M. Konop, D. Sulejczak, J. Czuwara, P. Kosson, A. Misicka, A. W. Lipkowski, L. Rudnicka, *Wound Repair Regen.* **2017**, *25*, 62.
- [49] R. C. de Guzman, J. M. Saul, M. D. Ellenburg, M. R. Merrill, H. B. Coan, T. L. Smith, M. E. Van Dyke, *Biomaterials* **2013**, *34*, 1644.
- [50] Z. Cheng, X. Chen, D. Zhai, F. Gao, T. Guo, W. Li, S. Hao, J. Ji, B. Wang, *J. Nanobiotechnol.* **2018**, *16*, 1.
- [51] G. Perotto, G. Sandri, C. Pignatelli, G. Milanese, A. Athanassiou, *J. Mater. Chem. B* **2019**, *7*, 4385.
- [52] G. J. Dias, P. Mahoney, N. A. Hung, L. A. Sharma, P. Kalita, R. A. Smith, R. J. Kelly, A. Ali, *J. Biomed. Mater. Res. B: Appl. Biomater.* **2017**, *105*, 2034.
- [53] Yamauchi K., Maniwa M., Mori T., *J. Biomater. Sci. Polym. Ed.* **1998**, *9*, 259.
- [54] S. Rodríguez, A. Frölich, *Laser Tech. J.* **2017**, *14*, 31.
- [55] K. Anusavice, C. Shen, H. R. Rawls, *Phillip's Science of dental materials*, Elsevier Health Sciences, St. Louis, MO, USA **2013**.
- [56] M.-N. Abdallah, S. D. Tran, G. Abughanam, M. Laurenti, D. Zuanazzi, M. A. Mezour, Y. Xiao, M. Cerruti, W. L. Siqueira, F. Tamimi, *Acta Biomater.* **2017**, *54*, 150.
- [57] J. D. Andrade, V. Hlady, *Biopolymers/Non-Exclusion HPLC*, Springer, Berlin, Heidelberg, Germany **1986**.
- [58] S. Winkler, H. R. Ortman, M. T. Ryzek, *J. Prosthet. Dent.* **1975**, *34*, 11.
- [59] N. Giovambattista, P. G. Debenedetti, P. J. Rossky, *Proc. Natl. Acad. Sci. USA* **2009**, *106*, 15181.
- [60] M. Zoccola, A. Montarsolo, A. Aluigi, A. Varesano, C. Vineis, C. Tonin, *e-Polymers* **2007**, *7*, 105.
- [61] H. Zhu, R. Li, X. Wu, K. Chen, J. Che, *Eur. Polym. J.* **2017**, *86*, 154.
- [62] S. Feroz, N. Muhammad, J. Ratnayake, G. Dias, *Bioact. Mater.* **2020**, *5*, 496.
- [63] M. M. Singer, R. S. Tjeerdema, *Rev. Environ. Contam. Toxicol.* **1993**, *133*, 95.
- [64] K. Katoh, M. Shibayama, T. Tanabe, K. Yamauchi, *Biomaterials* **2004**, *25*, 2265.
- [65] F. M. Herman, J. I. Kroschwitz, *Encyclopedia of polymer science and engineering*, Wiley, New York, NY, USA **1985**.
- [66] E. Ranjit, S. Hamlet, R. M. Love, *Surf. Coat. Technol.* **2023**, *462*, 129457.
- [67] E. Ranjit, S. Hamlet, R. George, A. Sharma, R. M. Love, *J. Sci. Adv. Mater. Devices* **2022**, *7*, 100398.
- [68] Y. Wang, H. Wang, T. Zhao, M. Nakagaki, *Biosci. Biotechnol. Biochem.* **2010**, *74*, 108.
- [69] A. Nussinovitch, *Hydrocolloid Applications*, Springer, New York, NY, USA **1998**.
- [70] J. Smart, I. Kellaway, H. Worthington, *J. Pharm. Pharmacol.* **1984**, *36*, 295.
- [71] M. Essendoubi, M. Meunier, A. Scandolera, C. Gobinet, M. Manfait, C. Lambert, D. Auriol, R. Reynaud, O. Piot, *Int. J. Cosmet. Sci.* **2019**, *41*, 203.
- [72] R. H. Wilson, H. B. Lewis, *J. Biol. Chem.* **1927**, *73*, 543.
- [73] J. Tonzetich, P. Johnson, *Arch. Oral Biol.* **1977**, *22*, 125.
- [74] B. Zappacosta, A. Manni, S. Persichilli, A. Boari, D. Scribano, A. Minucci, L. Raffaelli, B. Giardina, P. De Sole, *Clin. Biochem.* **2007**, *40*, 661.
- [75] D. C. Macintosh, M. Sutherland, *J. Prosthet. Dent.* **2004**, *91*, 289.
- [76] A. Gökaltun, Y. B. Kang, M. L. Yarmush, O. B. Usta, A. Asatekin, *Sci. Rep.* **2019**, *9*, 7377.
- [77] R. Norman, G. Stewart, D. Maroso, J. Gephart, B. Kohut, *Dent. Mater.* **1987**, *3*, 342.
- [78] L. Léger, C. Creton, *Philos. Trans. A. Math. Phys. Eng. Sci.* **2008**, *366*, 1425.
- [79] L. Amorós-Galicia, A. Nardi-Ricart, C. Verdugo-González, C. M. Arroyo-García, E. García-Montoya, P. Pérez-Lozano, J. M. Suñé-Negre, M. Suñé-Pou, *Pharmaceutics* **2022**, *14*, 1995.
- [80] C. B. Dayan, S. Chun, N. Krishna-Subbaiah, D. M. Drotlef, M. B. Akolpoglu, M. Sitti, *Adv. Mater.* **2021**, *33*, 2103826.
- [81] J. Kirfel, T. M. Magin, J. Reichelt, *Cell Mol. Life Sci.* **2003**, *60*, 56.
- [82] S. Tomblyn, E. L. Pettit Kneller, S. J. Walker, M. D. Ellenburg, C. J. Kowalczewski, M. Van Dyke, L. Burnett, J. M. Saul, *J. Biomed. Mater. Res., Part B: Appl. Biomater.* **2016**, *104*, 2016.
- [83] L. A. Pace, J. F. Plate, S. Mannava, J. C. Barnwell, L. A. Koman, Z. Li, T. L. Smith, M. Van Dyke, *Tissue Eng. Part A* **2014**, *20*, 507.

- [84] F. Tramacere, L. Beccai, M. Kuba, A. Gozzi, A. Bifone, B. Mazzolai, *PLoS One* **2013**, *8*, e65074.
- [85] G. L. Ellman Arch, *Biochem. Biophys.* **1959**, *82*, 70.
- [86] S. A. Mortazavi, J. D. Smart, *Int. J. Pharm.* **1995**, *116*, 223.
- [87] V. V. Khutoryanskiy, *Macromol. Biosci.* **2011**, *11*, 748.
- [88] Y. Jiang, K. T. Turner, *Extreme Mech. Lett.* **2016**, *9*, 119.
- [89] G. Ponchel, F. Touchard, D. Duchêne, N. A. Peppas, *J. Controlled Release* **1987**, *5*, 129.

## Supporting Information

### **Bioinspired Physico-Chemical Surface Modifications for the Development of Advanced Retentive Systems**

*Eda Dzinovic, Lauren Clark, Niktash Keyhani, Nora Al Morhiby, Paul Byford, Siyang Wang, Sara Gamea, Kenneth Chu, Elizabeth Wnuk, Yu Liu, Nicole Rosik, Finn Giuliani, Nicola M. Pugno, Zhenyu J. Zhang, Owen Addison & Sherif Elsharkawy\**

#### **This file includes:**

Figs. S1 to S18  
Tables S1 to S5  
Movies S1 to S4

#### **Other Supporting Information for this manuscript include the following:**

Movies S1 to S4

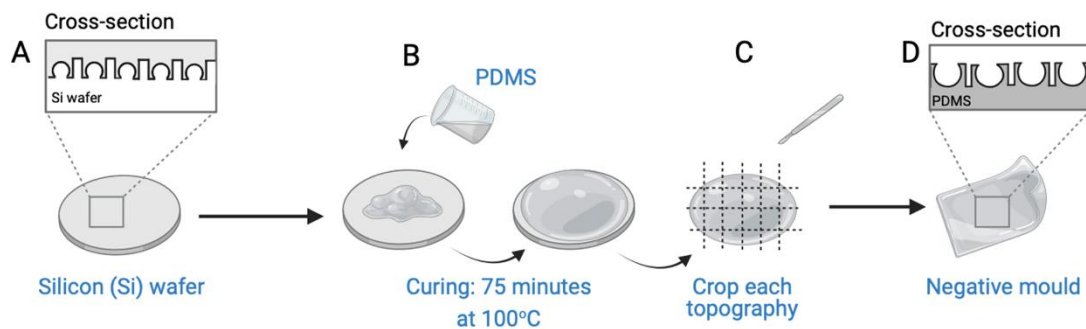


**Figure S1. Fabrication of negative PDMS moulds.** a) Si wafer with topographies. b) Si wafer covered evenly with PDMS mixture. The mixture was cured for 75 min at 100°C. c) The resulting topographies were cut out and stored as individual negative PDMS sheets. d) PDMS sheet with inverted patterns of the original Si wafer.

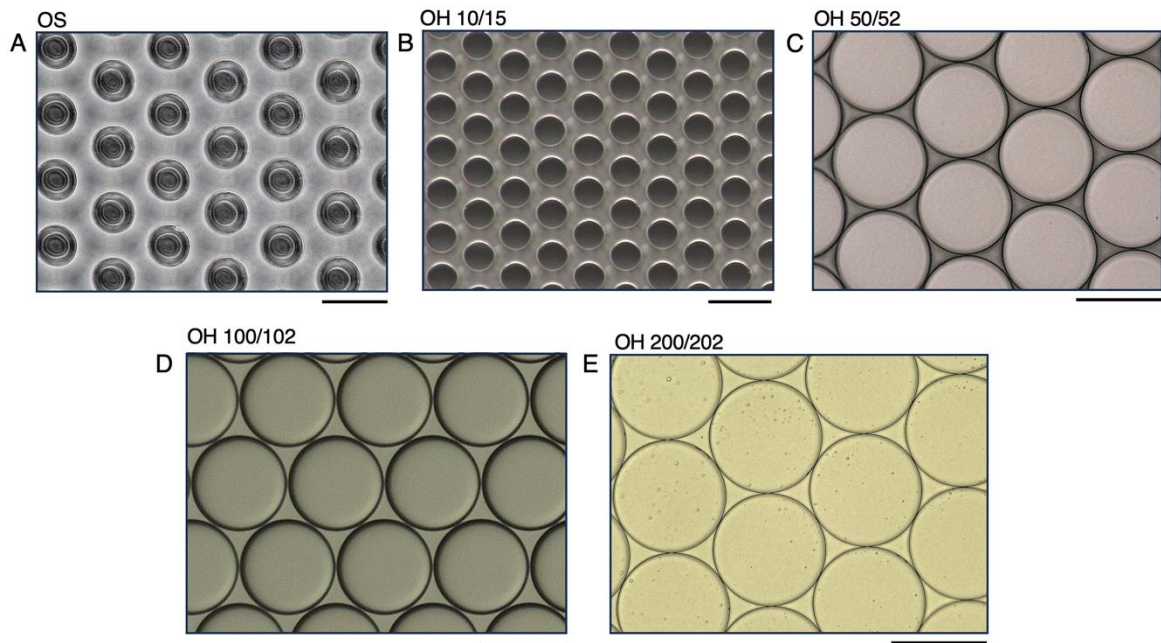


**Figure S2. A top-down view of negative PDMS moulds under digital microscope. a) OS (x2500). Scale bar, 20  $\mu\text{m}$ . b) OH 10/15 (x1000). Scale bar, 20  $\mu\text{m}$ . c) OH 50/52 (x1500). Scale bar, 50  $\mu\text{m}$ . d) OH 100/102 (x150). Scale bar, 100  $\mu\text{m}$ . e) OH 200/202 (x400). Scale bar, 200  $\mu\text{m}$ .**

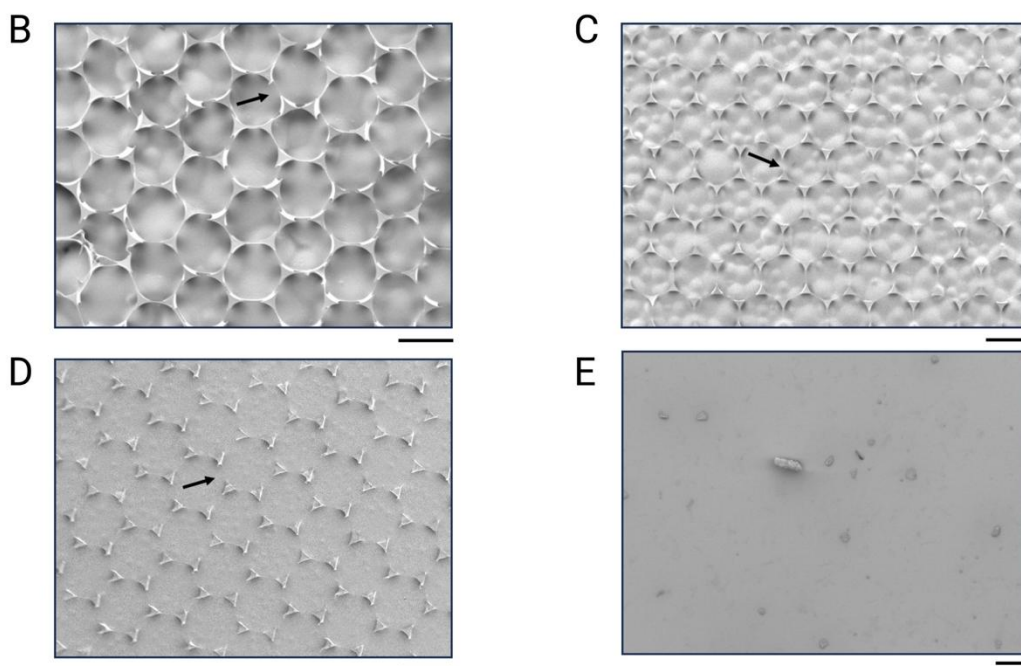
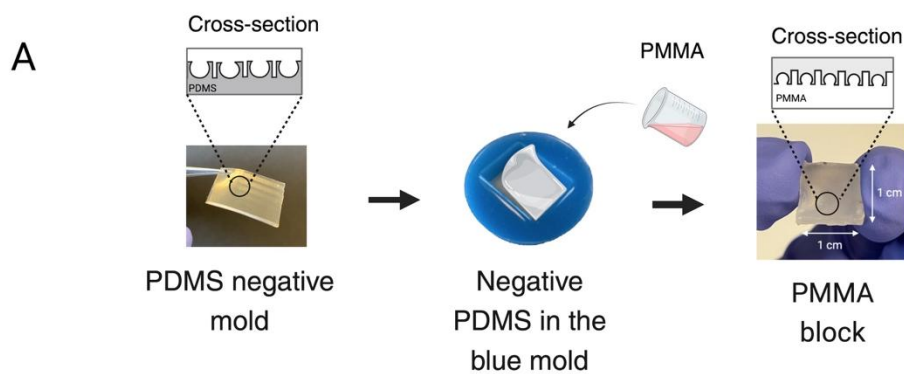


**Figure S3. Fabrication of acrylic blocks with topographies and SEM images of acrylic blocks with topographies (top-down view).** a) Negative PDMS mould with an inverted topography design. PDMS negative sheet is positioned at the base of a blue silicone mould and PMMA is poured onto the PDMS to obtain blocks in a size of 1 cm x 1 cm. b) OH 50/52 (x330). Scale bar, 50  $\mu\text{m}$ . c) OH 100/102 (x130). Scale bar, 100  $\mu\text{m}$ . d) OH 200/202 (x75). Scale bar, 200  $\mu\text{m}$ . e) Flat acrylic surface (x100). Scale bar, 100  $\mu\text{m}$ . Arrows indicate incomplete holes.

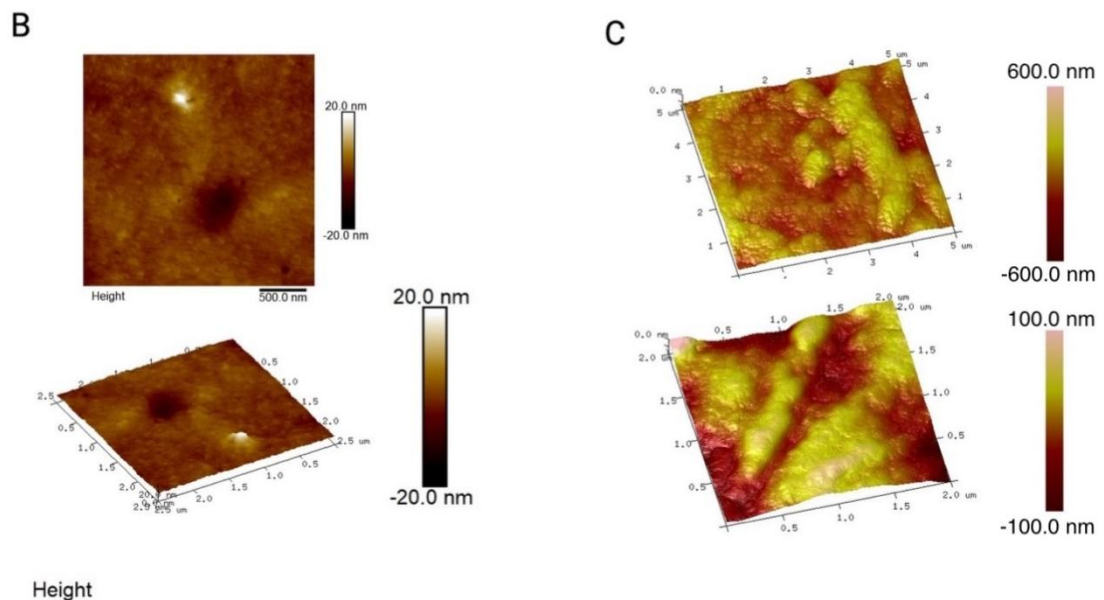
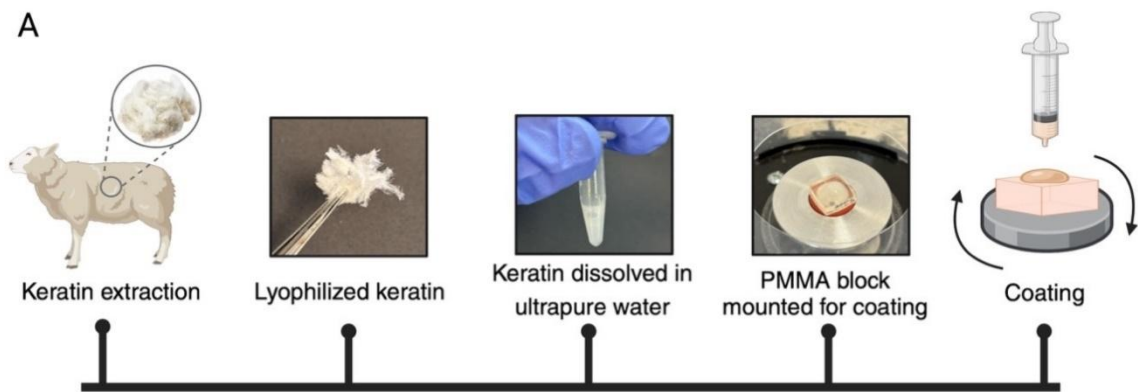


**Figure S4. Keratin extraction, spin coating, and surface characterization with atomic force microscopy (AFM).** a) After extraction from sheep's wool, lyophilized keratin powder was dissolved in ultrapure water at pH 7 and drop casted onto the surface of PMMA to perform the coating. b) Surface characterization of organic keratin with AFM prior to coating in liquid state. c) Rough surface depicts the state of keratin solution after drying and film assembly. The color bars indicate the differences in thickness.

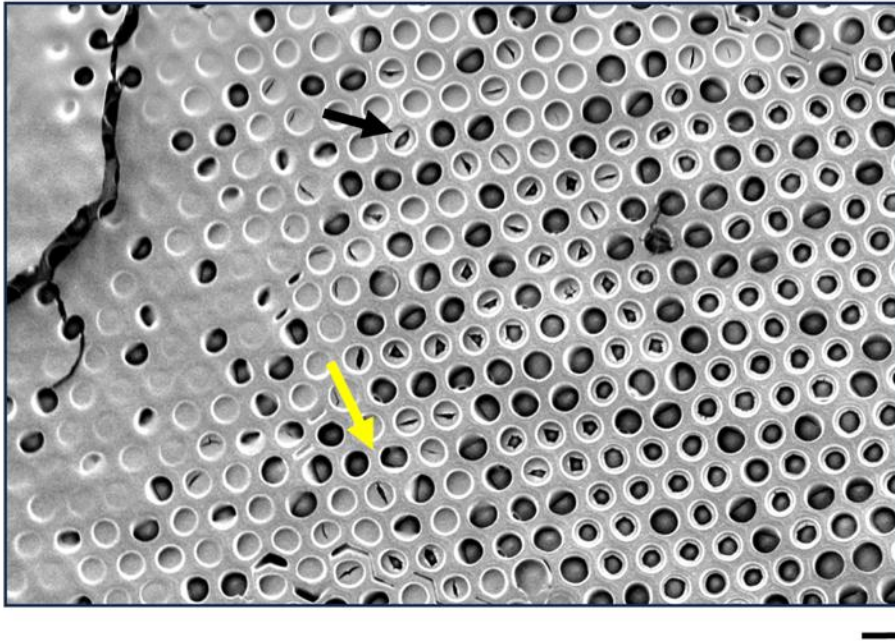


**Figure S5. SEM image of an OS acrylic block after keratin coating.** OS acrylic block coated with keratin that covers mainly the entrances of topographies as indicated with the black arrow. The yellow arrow shows the deposition of keratin between the holes (x370). Scale bar, 15  $\mu\text{m}$ .

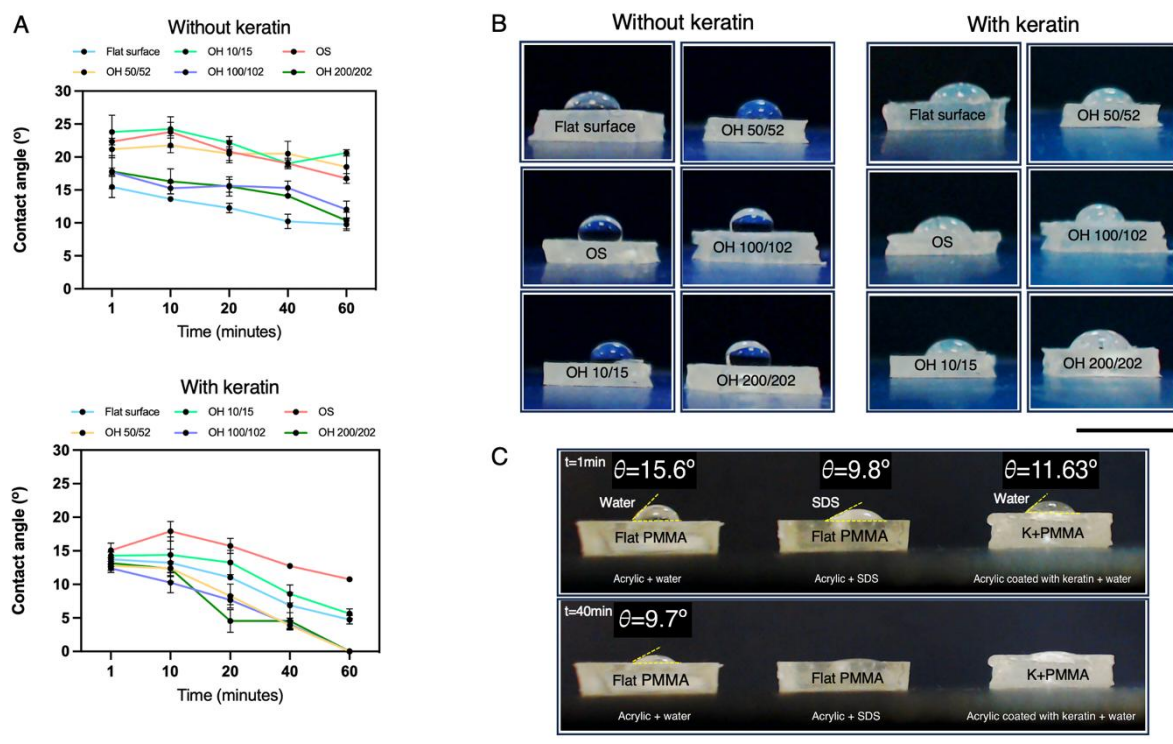


**Figure S6. Assessment of the static water contact angles (WCAs) on acrylic blocks. a)** WCA profiles without and with keratin coating ( $N = 3$ ). Quantification of contact angle values is represented on the graph as the means  $\pm$  standard deviation (error bars) for three independent experiments. **b)** Shapes of water droplets before and after keratin deposition on acrylic blocks ( $t = 1$  min). Scale bar, 1 cm. **c)** WCAs in the presence of SDS and keratin on acrylic blocks immediately after the droplet's deposition ( $t = 1$  min) and 40 minutes after ( $t = 40$  min) (K = keratin). Scale bar, 1 cm.

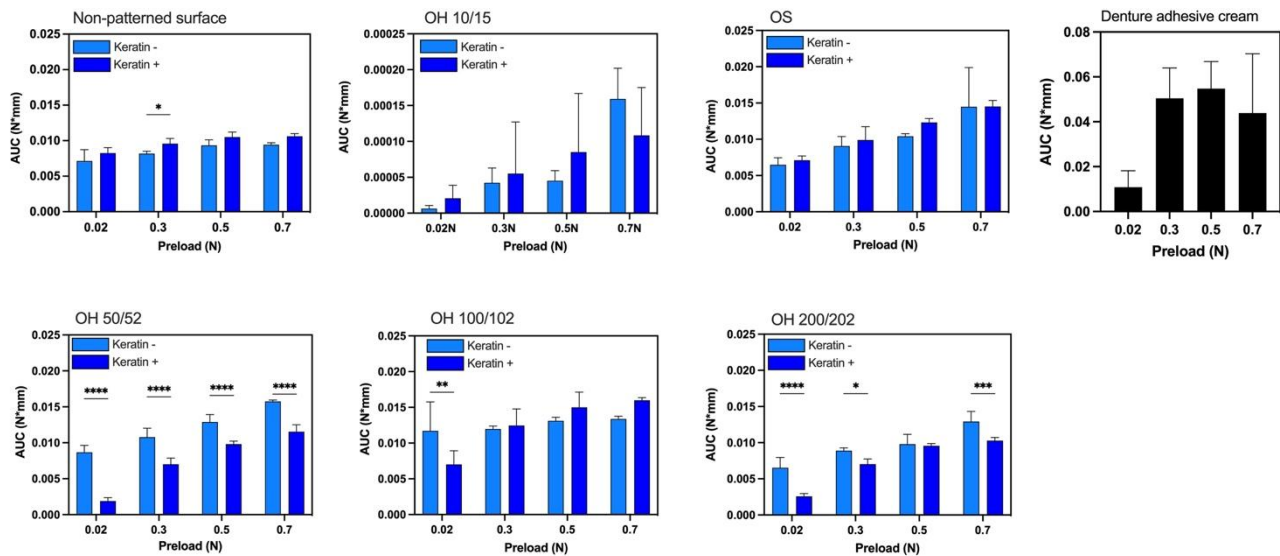


**Figure S7. Total work of adhesion profiles of patterned and non-patterned acrylic blocks.** Graphs depict the total work of adhesion for coated (+) and non-coated (-) acrylic blocks. All the error bars in the graphs represent standard deviations for the samples ( $N = 20$ ). Statistics were performed using a two-way ANOVA with a Šidák's post-test, \* $p < 0.05$ , \*\* $p < 0.01$ , \*\*\* $p < 0.001$ , \*\*\*\* $p < 0.0001$ .

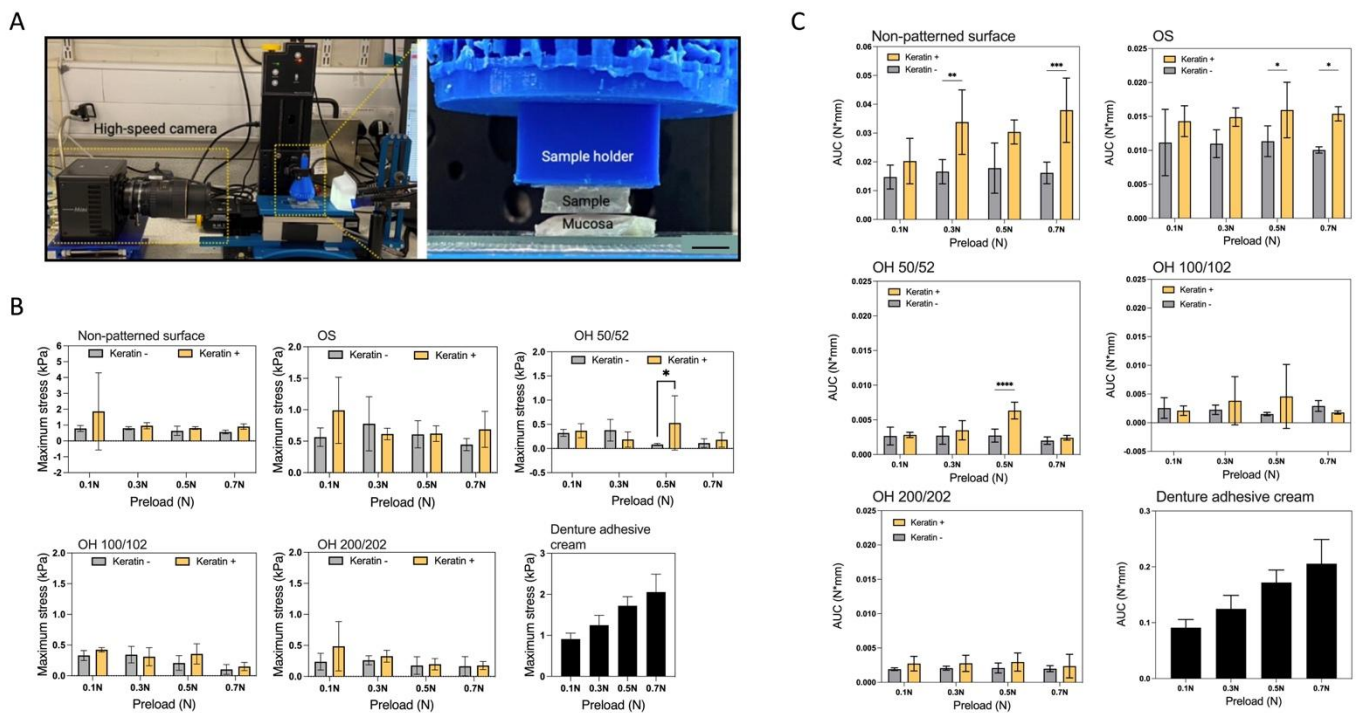


**Figure S8. Pull-off adhesion test with the lightweight tensile tester (force plate).** a) Setup for a pull-off adhesion test included the lightweight tensile testing machine and high-speed camera. Scale bar, 5 mm. b) Maximum stress profiles. c) Total work of adhesion profiles for topographies, with (+) and without (-) the hair keratin and the commercial denture adhesive. All the error bars in the graphs represent standard deviations for the samples ( $N = 20$ ). Statistics were performed using a two-way ANOVA with a Šidák's post-test, \* $p < 0.05$ , \*\* $p < 0.01$ , \*\*\* $p < 0.001$ , \*\*\*\* $p < 0.0001$ .

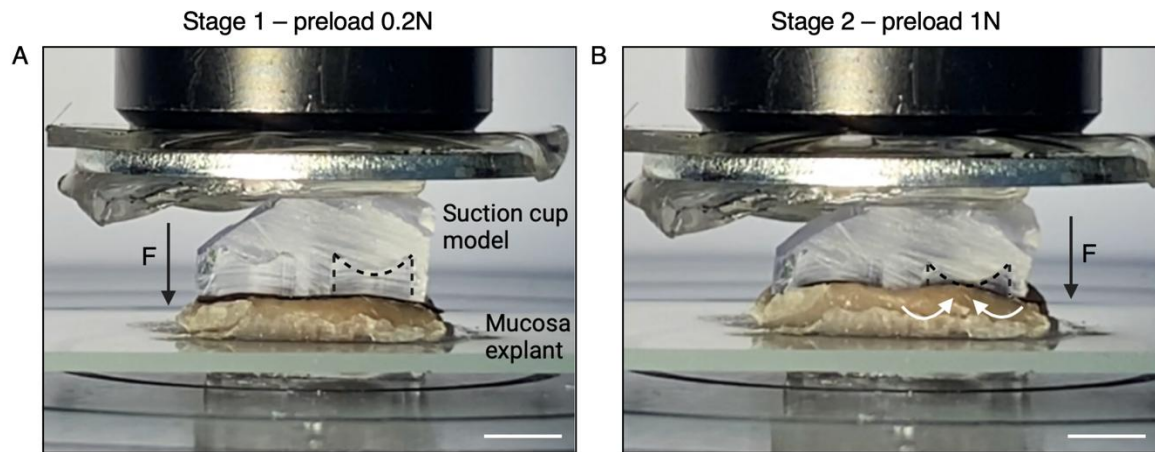


**Figure S9. Adhesion mechanism demonstrated with large 3D printed OS model.** a) Cross-sectioned large-scale OS model under negligible preload (0.2 N). Scale bar, 5 mm. b) Larger preload is applied (1 N). Although the higher preload brings surfaces closer, the protuberance prevents mucosa from entering the OS chamber. Scale bar, 5 mm.

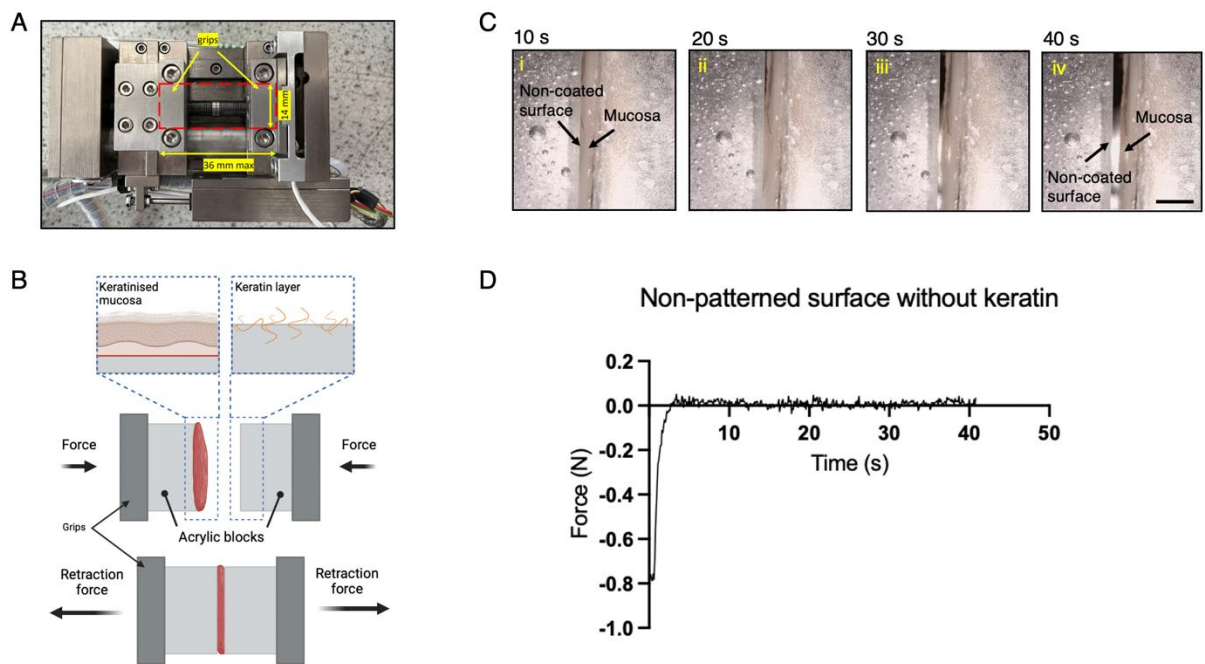


**Figure S10. Pull-off adhesion test with the micro tensile tester (Deben).** a) Specifications of a micro tensile tester. b) A schematic illustration depicts how the opposite ends of acrylic blocks are clamped by the grips. One surface (left acrylic block) contains keratinised mucosa while the other (right acrylic block) is coated with the keratin. c) Detachment of non-coated acrylic block from keratinised mucosa occurred without the formation of microfibrils at any time point. Scale bar, 5 mm. d) The graph for the non-coated acrylic block does not show the deflection as seen for a keratin-coated block in Figure 3e. Scale bar, 5 mm.

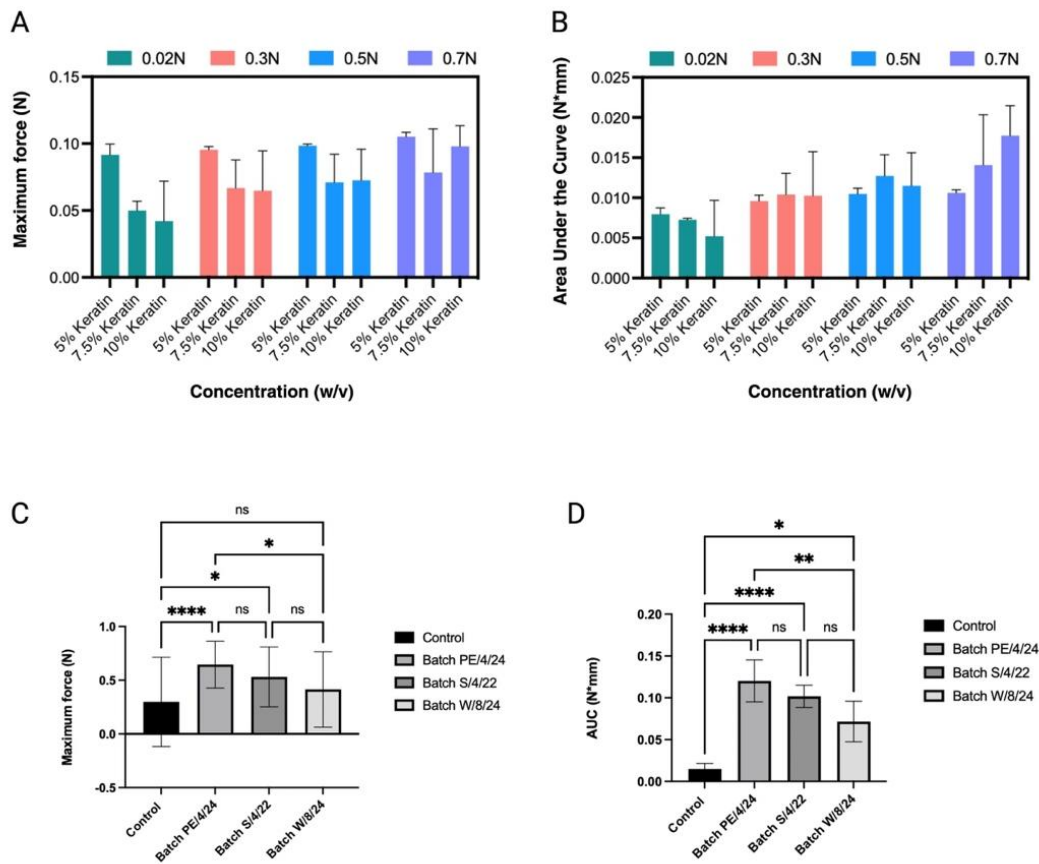


**Figure S11. Impact of different keratin concentrations and batch variability on the adhesion.** a) Maximum detachment force profiles. b) Area under the curve (AUC) represents the total work of adhesion profiles for the 5% w/v, 7.5% w/v, and 10% w/v keratin concentrations. Quantification of contact angle values is represented on the graph as the means  $\pm$  SD (error bars) ( $N = 20$  for each % w/v). c) Maximum detachment forces for 5% w/v keratin coatings obtained from different batches (preload = 1 N). All batches demonstrate higher detachment forces than the control without keratin coating. The differences between batches PE/4/24 and W/8/24 may be attributed to the manual procedures involved in the keratin extraction process d) Total work of adhesion profiles for 5% w/v keratin coatings and batch variability. All batches had significantly higher total work of adhesion compared to the non-coated control. Statistics were performed using a Kruskal Wallis test with a Dunn's post-test, \* $p < 0.05$ , \*\* $p < 0.01$ , \*\*\* $p < 0.001$ , \*\*\*\* $p < 0.0001$ .  $N = 15$ . Error bars on plotted graphs represent standard deviation (SD).

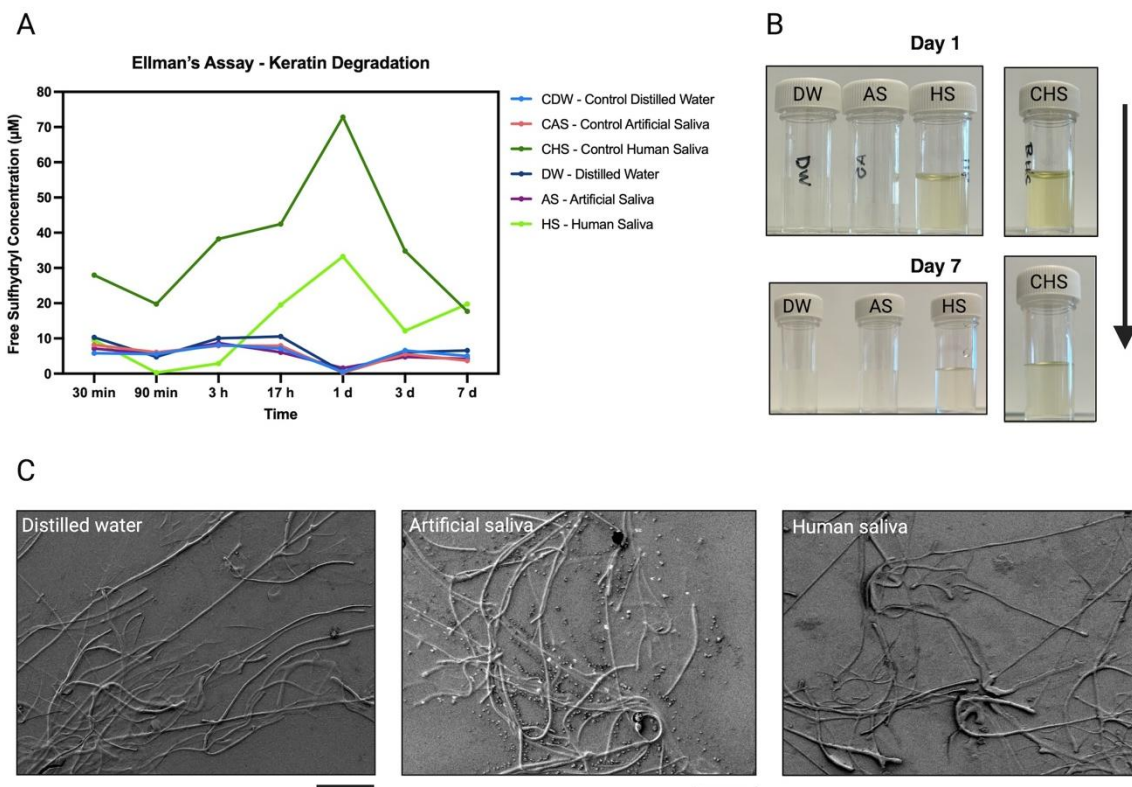


**Figure S12. Keratin coating degradation – Ellman's Assay.** a) The graph illustrates the variation in free sulfhydryl concentrations ( $\mu\text{M}$ ) over 7 days in different environments: controls in distilled water (CDW), artificial saliva (CAS), and human saliva (CHS); and the test groups (keratin-coated PMMA) in distilled water (DW), artificial saliva (AS), and human saliva (HS). b) The peaks for CHS and HS correlate to the changes in the color intensity of Ellman's solution when mixed with the unknown samples, observed on day 1. The intensity gradually diminished by day 7, which aligns with the results presented in the graph (a). c) SEM images of PMMA blocks incubated for 10 d in distilled water, artificial saliva, and human saliva, respectively, show that keratin coatings remain visible on the surface. Scale bars: 100  $\mu\text{m}$ .

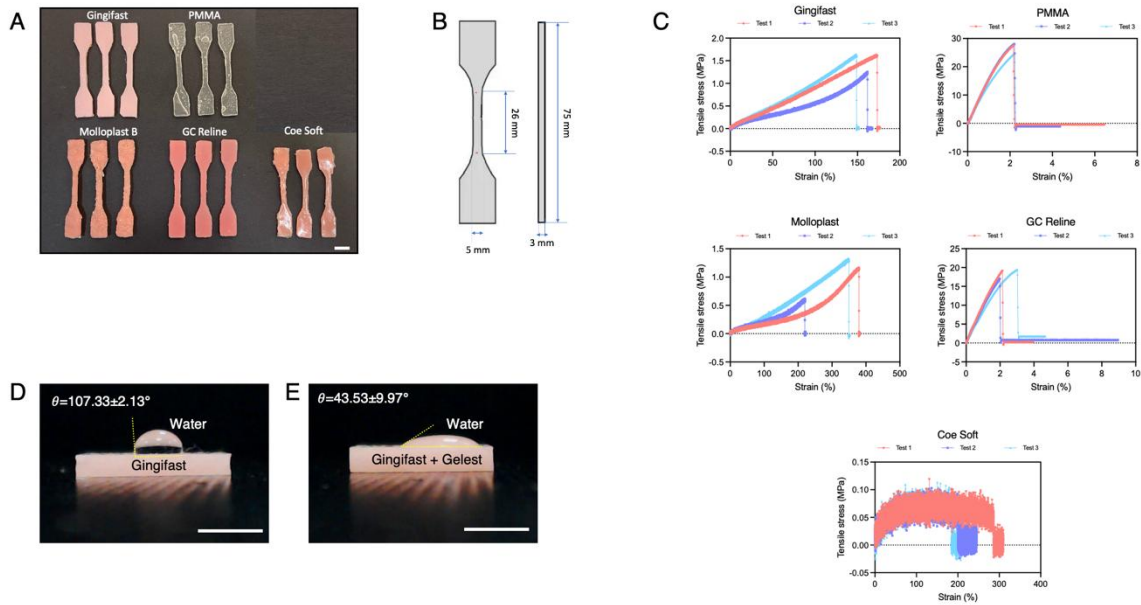


**Figure S13. Assessment of mechanical and surface properties of selected dental materials.** a) Dumbbell-shaped samples for the tensile test made of Gingifast, PMMA, Coe Soft, Molloplast B, and GC Reline. Scale bar, 15 mm. b) The schematic representation of the sample design and dimensions. c) Stress-strain curves are provided for each material. Coe Soft deforms irreversibly, Gingifast and Molloplast deform elastically, while PMMA and GC reline are brittle, resulting in steep resultant slopes. d) A water droplet on an unmodified/hydrophobic Gingifast surface ( $\theta = 107.3 \pm 2.13^\circ$ ). Scale bar, 10 mm. e) Hydrophilically modified Gingifast exhibits a significantly smaller water contact angle ( $\theta = 43.5 \pm 9.97^\circ$ ). Scale bar, 10 mm. All data are presented as the means  $\pm$  SD for independent experiments ( $N = 3$ ).

Sample	Young's modulus (MPa)	Mean (SD) (MPa)
<b>Gingifast 1</b>	0.99	1.31 ( $\pm$ 0.33)
<b>-II- 2</b>	1.65	
<b>-II- 3</b>	1.30	
<b>Molloplast 1</b>	0.69	0.55 ( $\pm$ 0.12)
<b>-II- 2</b>	0.5	
<b>-II- 3</b>	0.47	
<b>Acrylic 1</b>	1647.20	1616.51 ( $\pm$ 45.17)
<b>-II- 2</b>	1637.69	
<b>-II- 3</b>	1564.64	
<b>Coe Soft 1</b>	0.17	46.67 ( $\pm$ 59.83)
<b>-II- 2</b>	25.67	
<b>-II- 3</b>	114.17	
<b>GC reline 1</b>	1085.47	1050.15 ( $\pm$ 101.08)
<b>-II- 2</b>	1128.85	
<b>-II- 3</b>	936.15	

**Table S1. Young's moduli of dental materials selected for the tensile test.**

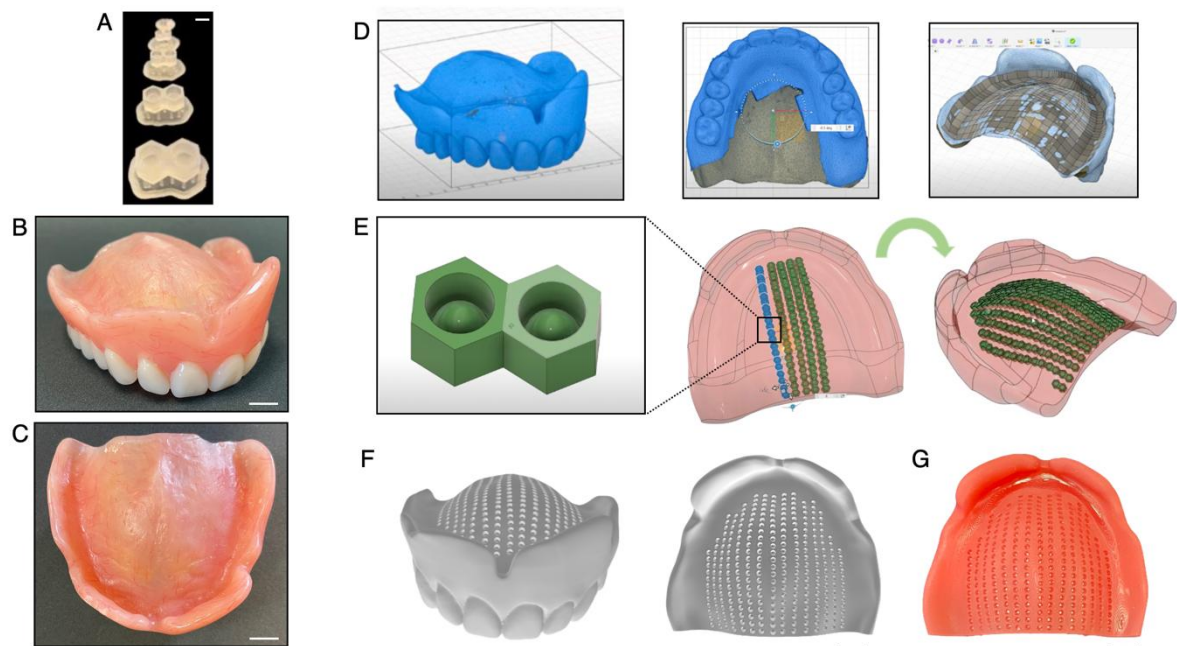


**Figure S14. Step-by-step design process of a denture with topographies on the fitting surface.** a) Individual topographies were printed to assess the resolution of a 3D printer. Scale bar, 1 mm. b) Conventional complete denture (front view). Scale bar, 8 mm. c) Conventional complete denture (top-down view). Scale bar, 8 mm. d) Conventional denture was scanned and converted to an STL file with minor adjustments in 3D CAM software. e) The STL file of an OS model was merged with the STL file of a denture. Topographies were positioned in an ordered manner until the whole palatal surface was covered. f) Final design – STL file of a bio-denture with topographies. Scale bar, 8 mm. g) Printed resin denture with topographies. Scale bar, 8 mm.

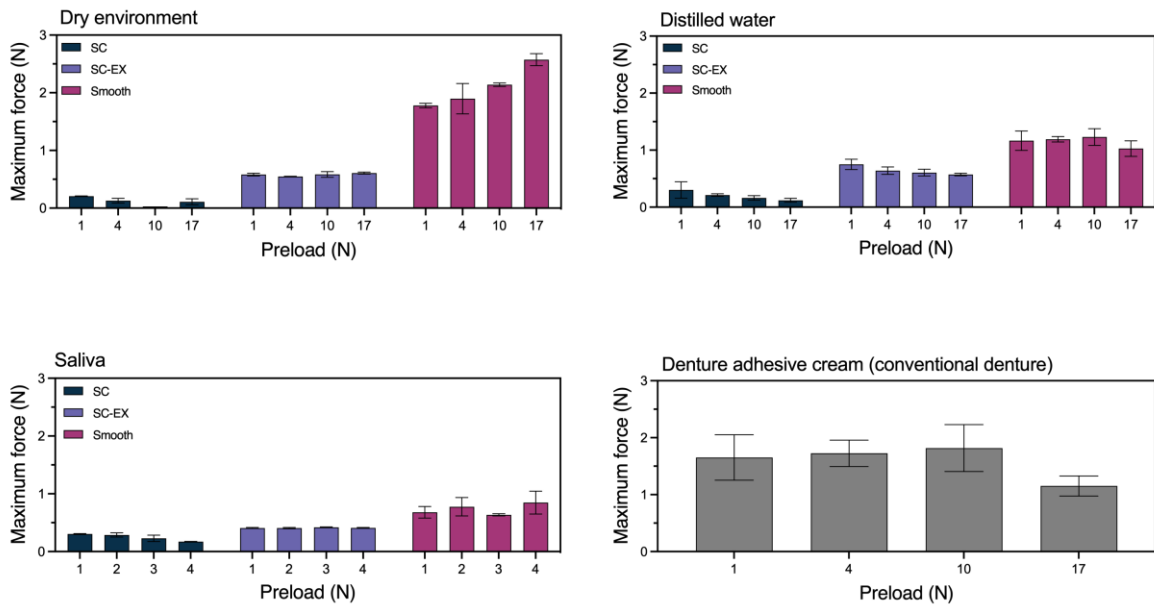


**Figure S15. Maximum detachment force values for dentures comprising topographies in soft material on the fitting surface across different environments.** All the error bars in the graphs represent standard deviations for the samples ( $N = 20$ ). Statistical analysis is provided in Supporting Information, Tables S2-S5.

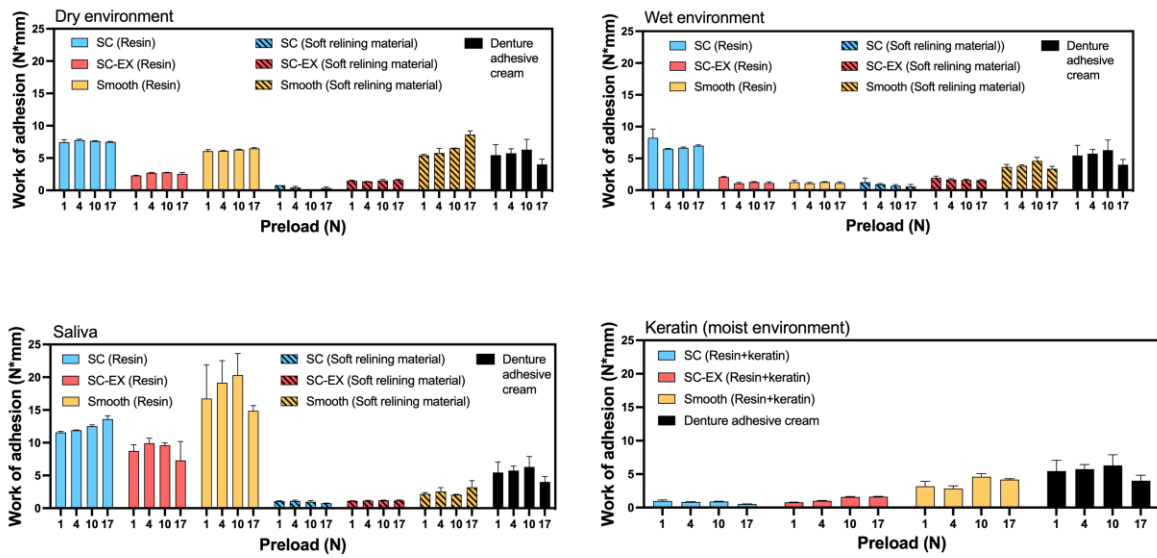
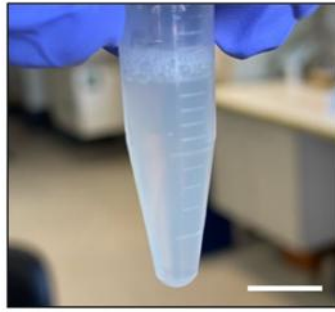


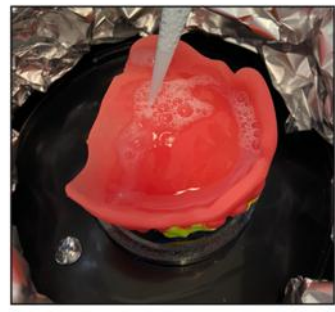
**Figure S16. Total work of adhesion for resin dentures, dentures with soft relining material, and denture adhesive cream.** All the error bars in the graphs represent standard deviations for the samples ( $N = 20$ ). Statistical analysis is provided in Supporting Information, Tables S2-S5.



Spin coater



5% w/v keratin solution



Denture coating

**Figure S17. Spin coating process of a denture with keratin solution.** The denture is affixed to the central, rotating part of a spin-coater. Subsequently, keratin solution is applied onto the denture surface before initiating the spinning. Scale bar, 1 cm.

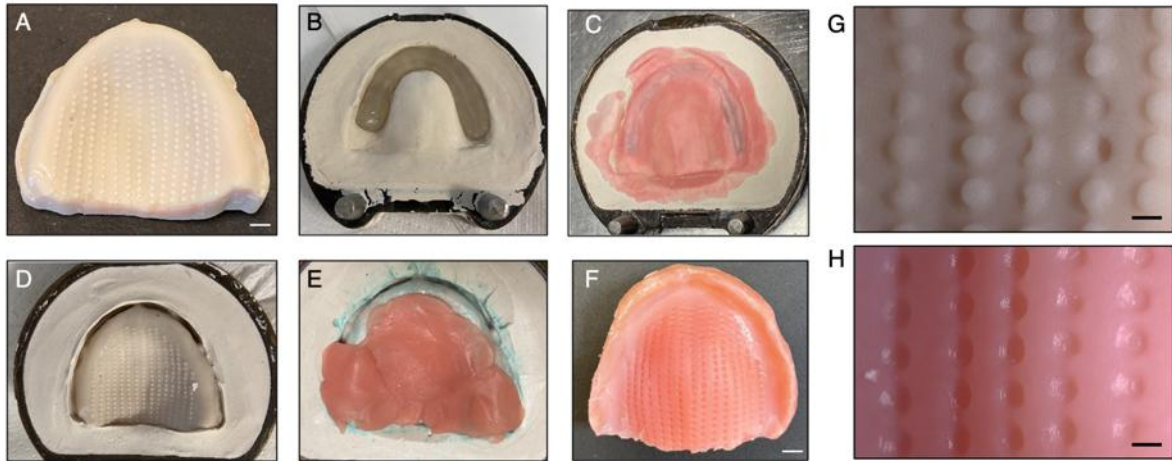


**Figure S18. Fabrication process of a denture with topographies embedded in soft relining material.** a) A resin maxillary cast. Scale bar, 5 mm. b) Dental arch with provisional teeth invested in a sectional flask. c) The dental arch is covered with a premixed cold-curing PMMA. d) Resin cast in a flask isolated to prevent sticking of a relining material e) Resin cast covered with soft relining material before application of the pressure. f) Denture with topographies in soft material. Scale bar, 5 mm. g) Surface of a negative resin cast with extruded cylinders. Scale bar, 1 mm. h) Denture with suction cups in soft material. Scale bar, 1 mm.

## DRY ENVIRONMENT

Tukey's multiple comparisons test	Mean Diff.	95.00% CI of diff.	Below threshold?	Summary	Adjusted P Value
Preload 1N					
SC (Resin) vs. SC-EX (Resin)	1.557	1.296 to 1.819	Yes	****	<0.0001
SC (Resin) vs. Smooth (Resin)	0.5658	0.3047 to 0.8269	Yes	****	<0.0001
SC (Resin) vs. SC (Molloplast®)	2.314	2.053 to 2.575	Yes	****	<0.0001
SC (Resin) vs. SC-EX (Molloplast®)	1.938	1.677 to 2.199	Yes	****	<0.0001
SC (Resin) vs. Smooth (Molloplast®)	0.742	0.4809 to 1.003	Yes	****	<0.0001
SC (Resin) vs. Fixodent®	0.868	0.6069 to 1.129	Yes	****	<0.0001
SC-EX (Resin) vs. Smooth (Resin)	-0.9916	-1.253 to -0.7305	Yes	****	<0.0001
SC-EX (Resin) vs. SC (Molloplast®)	0.7566	0.4954 to 1.018	Yes	****	<0.0001
SC-EX (Resin) vs. SC-EX (Molloplast®)	0.3806	0.1194 to 0.6417	Yes	***	0.0005
SC-EX (Resin) vs. Smooth (Molloplast®)	-0.8154	-1.077 to -0.5543	Yes	****	<0.0001
SC-EX (Resin) vs. Fixodent®	-0.6894	-0.9506 to -0.4283	Yes	****	<0.0001
Smooth (Resin) vs. SC (Molloplast®)	1.748	1.487 to 2.009	Yes	****	<0.0001
Smooth (Resin) vs. SC-EX (Molloplast®)	1.372	1.111 to 1.633	Yes	****	<0.0001
Smooth (Resin) vs. Smooth (Molloplast®)	0.1762	-0.08494 to 0.4373	No	ns	0.4044
Smooth (Resin) vs. Fixodent®	0.3022	0.04106 to 0.5633	Yes	*	0.0125
SC (Molloplast®) vs. SC-EX (Molloplast®)	-0.376	-0.6371 to -0.1149	Yes	***	0.0006
SC (Molloplast®) vs. Smooth (Molloplast®)	-1.572	-1.833 to -1.311	Yes	****	<0.0001
SC (Molloplast®) vs. Fixodent®	-1.446	-1.707 to -1.185	Yes	****	<0.0001
SC-EX (Molloplast®) vs. Smooth (Molloplast®)	-1.196	-1.457 to -0.9349	Yes	****	<0.0001
SC-EX (Molloplast®) vs. Fixodent®	-1.07	-1.331 to -0.8089	Yes	****	<0.0001

Smooth (Molloplast®) vs. Fixodent®	0.126	-0.1351 to 0.3871	No	ns	0.774

Preload 4N					
SC (Resin) vs. SC-EX (Resin)	1.44	1.179 to 1.701	Yes	****	<0.0001
SC (Resin) vs. Smooth (Resin)	0.5208	0.2597 to 0.7819	Yes	****	<0.0001
SC (Resin) vs. SC (Molloplast®)	2.292	2.031 to 2.553	Yes	****	<0.0001
SC (Resin) vs. SC-EX (Molloplast®)	1.874	1.613 to 2.135	Yes	****	<0.0001
SC (Resin) vs. Smooth (Molloplast®)	0.522	0.2609 to 0.7831	Yes	****	<0.0001
SC (Resin) vs. Fixodent®	0.694	0.4329 to 0.9551	Yes	****	<0.0001
SC-EX (Resin) vs. Smooth (Resin)	-0.9195	-1.181 to -0.6584	Yes	****	<0.0001
SC-EX (Resin) vs. SC (Molloplast®)	0.8517	0.5906 to 1.113	Yes	****	<0.0001
SC-EX (Resin) vs. SC-EX (Molloplast®)	0.4337	0.1726 to 0.6948	Yes	****	<0.0001
SC-EX (Resin) vs. Smooth (Molloplast®)	-0.9183	-1.179 to -0.6572	Yes	****	<0.0001
SC-EX (Resin) vs. Fixodent®	-0.7463	-1.007 to -0.4852	Yes	****	<0.0001
Smooth (Resin) vs. SC (Molloplast®)	1.771	1.510 to 2.032	Yes	****	<0.0001
Smooth (Resin) vs. SC-EX (Molloplast®)	1.353	1.092 to 1.614	Yes	****	<0.0001
Smooth (Resin) vs. Smooth (Molloplast®)	0.0012	-0.2599 to 0.2623	No	ns	>0.9999
Smooth (Resin) vs. Fixodent®	0.1732	-0.08794 to 0.4343	No	ns	0.4259
SC (Molloplast®) vs. SC-EX (Molloplast®)	-0.418	-0.6791 to -0.1569	Yes	****	<0.0001
SC (Molloplast®) vs. Smooth (Molloplast®)	-1.77	-2.031 to -1.509	Yes	****	<0.0001
SC (Molloplast®) vs. Fixodent®	-1.598	-1.859 to -1.337	Yes	****	<0.0001
SC-EX (Molloplast®) vs. Smooth (Molloplast®)	-1.352	-1.613 to -1.091	Yes	****	<0.0001
SC-EX (Molloplast®) vs. Fixodent®	-1.18	-1.441 to -0.9189	Yes	****	<0.0001

Smooth (Molloplast®) vs. Fixodent®	0.172	-0.08914 to 0.4331	No	ns	0.4346
------------------------------------	-------	--------------------	----	----	--------

Preload 10N					
SC (Resin) vs. SC-EX (Resin)	1.31	1.049 to 1.571	Yes	****	<0.0001
SC (Resin) vs. Smooth (Resin)	0.374	0.1129 to 0.6351	Yes	***	0.0007
SC (Resin) vs. SC (Molloplast®)	2.27	2.009 to 2.531	Yes	****	<0.0001
SC (Resin) vs. SC-EX (Molloplast®)	1.716	1.455 to 1.977	Yes	****	<0.0001
SC (Resin) vs. Smooth (Molloplast®)	0.16	-0.1011 to 0.4211	No	ns	0.5244
SC (Resin) vs. Fixodent®	0.482	0.2209 to 0.7431	Yes	****	<0.0001
SC-EX (Resin) vs. Smooth (Resin)	-0.9359	-1.197 to -0.6748	Yes	****	<0.0001
SC-EX (Resin) vs. SC (Molloplast®)	0.9601	0.6990 to 1.221	Yes	****	<0.0001
SC-EX (Resin) vs. SC-EX (Molloplast®)	0.4061	0.1450 to 0.6672	Yes	***	0.0002
SC-EX (Resin) vs. Smooth (Molloplast®)	-1.15	-1.411 to -0.8888	Yes	****	<0.0001
SC-EX (Resin) vs. Fixodent®	-0.8279	-1.089 to -0.5668	Yes	****	<0.0001
Smooth (Resin) vs. SC (Molloplast®)	1.896	1.635 to 2.157	Yes	****	<0.0001
Smooth (Resin) vs. SC-EX (Molloplast®)	1.342	1.081 to 1.603	Yes	****	<0.0001
Smooth (Resin) vs. Smooth (Molloplast®)	-0.214	-0.4751 to 0.04714	No	ns	0.184
Smooth (Resin) vs. Fixodent®	0.108	-0.1531 to 0.3691	No	ns	0.8761
SC (Molloplast®) vs. SC-EX (Molloplast®)	-0.554	-0.8151 to -0.2929	Yes	****	<0.0001
SC (Molloplast®) vs. Smooth (Molloplast®)	-2.11	-2.371 to -1.849	Yes	****	<0.0001
SC (Molloplast®) vs. Fixodent®	-1.788	-2.049 to -1.527	Yes	****	<0.0001
SC-EX (Molloplast®) vs. Smooth (Molloplast®)	-1.556	-1.817 to -1.295	Yes	****	<0.0001
SC-EX (Molloplast®) vs. Fixodent®	-1.234	-1.495 to -0.9729	Yes	****	<0.0001

Smooth (Molloplast®) vs. Fixodent®	0.322	0.06086 to 0.5831	Yes	**	0.006
------------------------------------	-------	-------------------	-----	----	-------

Preload 17N					
SC (Resin) vs. SC-EX (Resin)	1.326	1.065 to 1.587	Yes	****	<0.0001
SC (Resin) vs. Smooth (Resin)	0.3172	0.05606 to 0.5783	Yes	**	0.0072
SC (Resin) vs. SC (Molloplast®)	2.17	1.909 to 2.431	Yes	****	<0.0001
SC (Resin) vs. SC-EX (Molloplast®)	1.672	1.411 to 1.933	Yes	****	<0.0001
SC (Resin) vs. Smooth (Molloplast®)	-0.294	-0.5551 to -0.03286	Yes	*	0.0168
SC (Resin) vs. Fixodent®	1.128	0.8669 to 1.389	Yes	****	<0.0001
SC-EX (Resin) vs. Smooth (Resin)	-1.009	-1.270 to -0.7477	Yes	****	<0.0001
SC-EX (Resin) vs. SC (Molloplast®)	0.844	0.5828 to 1.105	Yes	****	<0.0001
SC-EX (Resin) vs. SC-EX (Molloplast®)	0.346	0.08482 to 0.6071	Yes	**	0.0023
SC-EX (Resin) vs. Smooth (Molloplast®)	-1.62	-1.881 to -1.359	Yes	****	<0.0001
SC-EX (Resin) vs. Fixodent®	-0.198	-0.4592 to 0.06310	No	ns	0.2644
Smooth (Resin) vs. SC (Molloplast®)	1.853	1.592 to 2.114	Yes	****	<0.0001
Smooth (Resin) vs. SC-EX (Molloplast®)	1.355	1.094 to 1.616	Yes	****	<0.0001
Smooth (Resin) vs. Smooth (Molloplast®)	-0.6112	-0.8723 to -0.3501	Yes	****	<0.0001
Smooth (Resin) vs. Fixodent®	0.8108	0.5497 to 1.072	Yes	****	<0.0001
SC (Molloplast®) vs. SC-EX (Molloplast®)	-0.498	-0.7591 to -0.2369	Yes	****	<0.0001
SC (Molloplast®) vs. Smooth (Molloplast®)	-2.464	-2.725 to -2.203	Yes	****	<0.0001
SC (Molloplast®) vs. Fixodent®	-1.042	-1.303 to -0.7809	Yes	****	<0.0001
SC-EX (Molloplast®) vs. Smooth (Molloplast®)	-1.966	-2.227 to -1.705	Yes	****	<0.0001

SC-EX (Molloplast®) vs. Fixodent®	-0.544	-0.8051 to -0.2829	Yes	****	<0.0001
Smooth (Molloplast®) vs. Fixodent®	1.422	1.161 to 1.683	Yes	****	<0.0001

**Table S2. Statistical analysis and Tukey's multiple comparisons tests for dentures' detachment forces across different preloads in dry environment.**

## WET ENVIRONEMENT

Tukey's multiple comparisons test	Mean Diff.	95.00% CI of diff.	Below threshold?	Summary	Adjusted P Value
Preload 1N					
SC (Resin) vs. SC-EX (Resin)	1.401	1.047 to 1.755	Yes	****	<0.0001
SC (Resin) vs. Smooth (Resin)	1.786	1.432 to 2.140	Yes	****	<0.0001
SC (Resin) vs. SC (Molloplast®)	1.939	1.585 to 2.293	Yes	****	<0.0001
SC (Resin) vs. SC-EX (Molloplast®)	1.49	1.136 to 1.844	Yes	****	<0.0001
SC (Resin) vs. Smooth (Molloplast®)	1.074	0.7201 to 1.428	Yes	****	<0.0001
SC (Resin) vs. Fixodent®	0.588	0.2341 to 0.9419	Yes	****	<0.0001
SC-EX (Resin) vs. Smooth (Resin)	0.3849	0.03109 to 0.7388	Yes	*	0.0237
SC-EX (Resin) vs. SC (Molloplast®)	0.538	0.1841 to 0.8918	Yes	***	0.0003
SC-EX (Resin) vs. SC-EX (Molloplast®)	0.08878	-0.2651 to 0.4426	No	ns	0.9887
SC-EX (Resin) vs. Smooth (Molloplast®)	-0.327	-0.6809 to 0.02684	No	ns	0.09
SC-EX (Resin) vs. Fixodent®	-0.813	-1.167 to -0.4592	Yes	****	<0.0001
Smooth (Resin) vs. SC (Molloplast®)	0.153	-0.2008 to 0.5069	No	ns	0.8513
Smooth (Resin) vs. SC-EX (Molloplast®)	-0.2962	-0.6500 to 0.05769	No	ns	0.1646
Smooth (Resin) vs. Smooth (Molloplast®)	-0.712	-1.066 to -0.3581	Yes	****	<0.0001
Smooth (Resin) vs. Fixodent®	-1.198	-1.552 to -0.8441	Yes	****	<0.0001
SC (Molloplast®) vs. SC-EX (Molloplast®)	-0.4492	-0.8031 to -0.09534	Yes	**	0.0041
SC (Molloplast®) vs. Smooth (Molloplast®)	-0.865	-1.219 to -0.5111	Yes	****	<0.0001
SC (Molloplast®) vs. Fixodent®	-1.351	-1.705 to -0.9971	Yes	****	<0.0001
SC-EX (Molloplast®) vs. Smooth (Molloplast®)	-0.4158	-0.7697 to -0.06194	Yes	*	0.0106
SC-EX (Molloplast®) vs. Fixodent®	-0.9018	-1.256 to -0.5479	Yes	****	<0.0001
Smooth (Molloplast®) vs. Fixodent®	-0.486	-0.8399 to -0.1321	Yes	**	0.0014

Preload 4N					
SC (Resin) vs. SC-EX (Resin)	1.42	1.066 to 1.774	Yes	****	<0.0001
SC (Resin) vs. Smooth (Resin)	1.42	1.066 to 1.774	Yes	****	<0.0001
SC (Resin) vs. SC (Molloplast®)	1.628	1.274 to 1.982	Yes	****	<0.0001
SC (Resin) vs. SC-EX (Molloplast®)	1.2	0.8461 to 1.554	Yes	****	<0.0001
SC (Resin) vs. Smooth (Molloplast®)	0.6492	0.2953 to 1.003	Yes	****	<0.0001
SC (Resin) vs. Fixodent®	0.114	-0.2399 to 0.4679	No	ns	0.9599
SC-EX (Resin) vs. Smooth (Resin)	0	-0.3539 to 0.3539	No	ns	>0.9999
SC-EX (Resin) vs. SC (Molloplast®)	0.2077	-0.1462 to 0.5615	No	ns	0.5762
SC-EX (Resin) vs. SC-EX (Molloplast®)	-0.2203	-0.5742 to 0.1335	No	ns	0.5046
SC-EX (Resin) vs. Smooth (Molloplast®)	-0.7711	-1.125 to -0.4173	Yes	****	<0.0001
SC-EX (Resin) vs. Fixodent®	-1.306	-1.660 to -0.9525	Yes	****	<0.0001
Smooth (Resin) vs. SC (Molloplast®)	0.2077	-0.1462 to 0.5615	No	ns	0.5762
Smooth (Resin) vs. SC-EX (Molloplast®)	-0.2203	-0.5742 to 0.1335	No	ns	0.5046
Smooth (Resin) vs. Smooth (Molloplast®)	-0.7711	-1.125 to -0.4173	Yes	****	<0.0001
Smooth (Resin) vs. Fixodent®	-1.306	-1.660 to -0.9525	Yes	****	<0.0001
SC (Molloplast®) vs. SC-EX (Molloplast®)	-0.428	-0.7819 to -0.07414	Yes	**	0.0076
SC (Molloplast®) vs. Smooth (Molloplast®)	-0.9788	-1.333 to -0.6249	Yes	****	<0.0001
SC (Molloplast®) vs. Fixodent®	-1.514	-1.868 to -1.160	Yes	****	<0.0001
SC-EX (Molloplast®) vs. Smooth (Molloplast®)	-0.5508	-0.9047 to -0.1969	Yes	***	0.0002
SC-EX (Molloplast®) vs. Fixodent®	-1.086	-1.440 to -0.7321	Yes	****	<0.0001
Smooth (Molloplast®) vs. Fixodent®	-0.5352	-0.8891 to -0.1813	Yes	***	0.0003

Preload 10N					
SC (Resin) vs. SC-EX (Resin)	1.438	1.084 to 1.792	Yes	****	<0.0001
SC (Resin) vs. Smooth (Resin)	1.438	1.084 to 1.792	Yes	****	<0.0001
SC (Resin) vs. SC (Molloplast®)	1.758	1.404 to 2.112	Yes	****	<0.0001
SC (Resin) vs. SC-EX (Molloplast®)	1.314	0.9601 to 1.668	Yes	****	<0.0001
SC (Resin) vs. Smooth (Molloplast®)	0.69	0.3361 to 1.044	Yes	****	<0.0001
SC (Resin) vs. Fixodent®	0.102	-0.2519 to 0.4559	No	ns	0.9769
SC-EX (Resin) vs. Smooth (Resin)	0	-0.3539 to 0.3539	No	ns	>0.9999
SC-EX (Resin) vs. SC (Molloplast®)	0.3198	-0.03402 to 0.6737	No	ns	0.1043
SC-EX (Resin) vs. SC-EX (Molloplast®)	-0.1242	-0.4780 to 0.2297	No	ns	0.94
SC-EX (Resin) vs. Smooth (Molloplast®)	-0.7482	-1.102 to -0.3943	Yes	****	<0.0001
SC-EX (Resin) vs. Fixodent®	-1.336	-1.690 to -0.9823	Yes	****	<0.0001
Smooth (Resin) vs. SC (Molloplast®)	0.3198	-0.03402 to 0.6737	No	ns	0.1043
Smooth (Resin) vs. SC-EX (Molloplast®)	-0.1242	-0.4780 to 0.2297	No	ns	0.94
Smooth (Resin) vs. Smooth (Molloplast®)	-0.7482	-1.102 to -0.3943	Yes	****	<0.0001
Smooth (Resin) vs. Fixodent®	-1.336	-1.690 to -0.9823	Yes	****	<0.0001
SC (Molloplast®) vs. SC-EX (Molloplast®)	-0.444	-0.7979 to -0.09014	Yes	**	0.0048
SC (Molloplast®) vs. Smooth (Molloplast®)	-1.068	-1.422 to -0.7141	Yes	****	<0.0001
SC (Molloplast®) vs. Fixodent®	-1.656	-2.010 to -1.302	Yes	****	<0.0001
SC-EX (Molloplast®) vs. Smooth (Molloplast®)	-0.624	-0.9779 to -0.2701	Yes	****	<0.0001
SC-EX (Molloplast®) vs. Fixodent®	-1.212	-1.566 to -0.8581	Yes	****	<0.0001
Smooth (Molloplast®) vs. Fixodent®	-0.588	-0.9419 to -0.2341	Yes	****	<0.0001

Preload 17N					
SC (Resin) vs. SC-EX (Resin)	1.582	1.228 to 1.936	Yes	****	<0.0001
SC (Resin) vs. Smooth (Resin)	1.582	1.228 to 1.936	Yes	****	<0.0001
SC (Resin) vs. SC (Molloplast®)	1.88	1.526 to 2.234	Yes	****	<0.0001
SC (Resin) vs. SC-EX (Molloplast®)	1.428	1.074 to 1.782	Yes	****	<0.0001
SC (Resin) vs. Smooth (Molloplast®)	0.9726	0.6187 to 1.326	Yes	****	<0.0001
SC (Resin) vs. Fixodent®	0.848	0.4941 to 1.202	Yes	****	<0.0001
SC-EX (Resin) vs. Smooth (Resin)	0	-0.3539 to 0.3539	No	ns	>0.9999
SC-EX (Resin) vs. SC (Molloplast®)	0.2977	-0.05620 to 0.6515	No	ns	0.1602
SC-EX (Resin) vs. SC-EX (Molloplast®)	-0.1543	-0.5082 to 0.1995	No	ns	0.8461
SC-EX (Resin) vs. Smooth (Molloplast®)	-0.6097	-0.9636 to -0.2559	Yes	****	<0.0001
SC-EX (Resin) vs. Fixodent®	-0.7343	-1.088 to -0.3805	Yes	****	<0.0001
Smooth (Resin) vs. SC (Molloplast®)	0.2977	-0.05620 to 0.6515	No	ns	0.1602
Smooth (Resin) vs. SC-EX (Molloplast®)	-0.1543	-0.5082 to 0.1995	No	ns	0.8461
Smooth (Resin) vs. Smooth (Molloplast®)	-0.6097	-0.9636 to -0.2559	Yes	****	<0.0001
Smooth (Resin) vs. Fixodent®	-0.7343	-1.088 to -0.3805	Yes	****	<0.0001
SC (Molloplast®) vs. SC-EX (Molloplast®)	-0.452	-0.8059 to -0.09814	Yes	**	0.0038
SC (Molloplast®) vs. Smooth (Molloplast®)	-0.9074	-1.261 to -0.5535	Yes	****	<0.0001
SC (Molloplast®) vs. Fixodent®	-1.032	-1.386 to -0.6781	Yes	****	<0.0001
SC-EX (Molloplast®) vs. Smooth (Molloplast®)	-0.4554	-0.8093 to -0.1015	Yes	**	0.0034
SC-EX (Molloplast®) vs. Fixodent®	-0.58	-0.9339 to -0.2261	Yes	****	<0.0001
Smooth (Molloplast®) vs. Fixodent®	-0.1246	-0.4785 to 0.2293	No	ns	0.939

**Table S3. Statistical analysis and Tukey's multiple comparisons tests for dentures' detachment forces across different preloads in wet environment.**

**SALIVARY-BASED ENVIRONMENT**

Tukey's multiple comparisons test	Mean Diff.	95.00% CI of diff.	Below threshold?	Summary	Adjusted P Value
Preload 1N					
SC (Resin) vs. SC-EX (Resin)	-0.3204	-0.6285 to -0.01234	Yes	*	0.0359
SC (Resin) vs. Smooth (Resin)	0.6872	0.3792 to 0.9953	Yes	****	<0.0001
SC (Resin) vs. SC (Molloplast®)	1.199	0.8909 to 1.507	Yes	****	<0.0001
SC (Resin) vs. SC-EX (Molloplast®)	1.094	0.7861 to 1.402	Yes	****	<0.0001
SC (Resin) vs. Smooth (Molloplast®)	0.8222	0.5141 to 1.130	Yes	****	<0.0001
SC (Resin) vs. Fixodent®	-0.1498	-0.4579 to 0.1583	No	ns	0.7675
SC-EX (Resin) vs. Smooth (Resin)	1.008	0.6996 to 1.316	Yes	****	<0.0001
SC-EX (Resin) vs. SC (Molloplast®)	1.519	1.211 to 1.827	Yes	****	<0.0001
SC-EX (Resin) vs. SC-EX (Molloplast®)	1.415	1.107 to 1.723	Yes	****	<0.0001
SC-EX (Resin) vs. Smooth (Molloplast®)	1.143	0.8345 to 1.451	Yes	****	<0.0001
SC-EX (Resin) vs. Fixodent®	0.1706	-0.1375 to 0.4787	No	ns	0.642
Smooth (Resin) vs. SC (Molloplast®)	0.5118	0.2037 to 0.8198	Yes	****	<0.0001
Smooth (Resin) vs. SC-EX (Molloplast®)	0.407	0.09890 to 0.7150	Yes	**	0.0024
Smooth (Resin) vs. Smooth (Molloplast®)	0.135	-0.1731 to 0.4430	No	ns	0.8434
Smooth (Resin) vs. Fixodent®	-0.837	-1.145 to -0.5290	Yes	****	<0.0001
SC (Molloplast®) vs. SC-EX (Molloplast®)	-0.1048	-0.4129 to 0.2033	No	ns	0.9481
SC (Molloplast®) vs. Smooth (Molloplast®)	-0.3768	-0.6849 to -0.06874	Yes	**	0.0066
SC (Molloplast®) vs. Fixodent®	-1.349	-1.657 to -1.041	Yes	****	<0.0001
SC-EX (Molloplast®) vs. Smooth (Molloplast®)	-0.272	-0.5801 to 0.03606	No	ns	0.1209
SC-EX (Molloplast®) vs. Fixodent®	-1.244	-1.552 to -0.9359	Yes	****	<0.0001
Smooth (Molloplast®) vs. Fixodent®	-0.972	-1.280 to -0.6639	Yes	****	<0.0001

--	--	--	--	--	--

Preload 4N					
SC (Resin) vs. SC-EX (Resin)	-0.4986	-0.8067 to -0.1905	Yes	****	<0.0001
SC (Resin) vs. Smooth (Resin)	0.6335	0.3255 to 0.9416	Yes	****	<0.0001
SC (Resin) vs. SC (Molloplast®)	1.346	1.038 to 1.654	Yes	****	<0.0001
SC (Resin) vs. SC-EX (Molloplast®)	1.228	0.9197 to 1.536	Yes	****	<0.0001
SC (Resin) vs. Smooth (Molloplast®)	0.8578	0.5497 to 1.166	Yes	****	<0.0001
SC (Resin) vs. Fixodent®	-0.0922	-0.4003 to 0.2159	No	ns	0.9721
SC-EX (Resin) vs. Smooth (Resin)	1.132	0.8241 to 1.440	Yes	****	<0.0001
SC-EX (Resin) vs. SC (Molloplast®)	1.845	1.537 to 2.153	Yes	****	<0.0001
SC-EX (Resin) vs. SC-EX (Molloplast®)	1.726	1.418 to 2.034	Yes	****	<0.0001
SC-EX (Resin) vs. Smooth (Molloplast®)	1.356	1.048 to 1.664	Yes	****	<0.0001
SC-EX (Resin) vs. Fixodent®	0.4064	0.09834 to 0.7145	Yes	**	0.0025
Smooth (Resin) vs. SC (Molloplast®)	0.7127	0.4046 to 1.021	Yes	****	<0.0001
Smooth (Resin) vs. SC-EX (Molloplast®)	0.5943	0.2862 to 0.9023	Yes	****	<0.0001
Smooth (Resin) vs. Smooth (Molloplast®)	0.2243	-0.08380 to 0.5323	No	ns	0.3115
Smooth (Resin) vs. Fixodent®	-0.7257	-1.034 to -0.4177	Yes	****	<0.0001
SC (Molloplast®) vs. SC-EX (Molloplast®)	-0.1184	-0.4265 to 0.1897	No	ns	0.9095
SC (Molloplast®) vs. Smooth (Molloplast®)	-0.4884	-0.7965 to -0.1803	Yes	***	0.0001
SC (Molloplast®) vs. Fixodent®	-1.438	-1.746 to -1.130	Yes	****	<0.0001
SC-EX (Molloplast®) vs. Smooth (Molloplast®)	-0.37	-0.6781 to -0.06194	Yes	**	0.0082
SC-EX (Molloplast®) vs. Fixodent®	-1.32	-1.628 to -1.012	Yes	****	<0.0001
Smooth (Molloplast®) vs. Fixodent®	-0.95	-1.258 to -0.6419	Yes	****	<0.0001

Preload 10N					
SC (Resin) vs. SC-EX (Resin)	-0.414	-0.7221 to -0.1059	Yes	**	0.0019
SC (Resin) vs. Smooth (Resin)	0.9042	0.5961 to 1.212	Yes	****	<0.0001
SC (Resin) vs. SC (Molloplast®)	1.559	1.251 to 1.867	Yes	****	<0.0001
SC (Resin) vs. SC-EX (Molloplast®)	1.369	1.061 to 1.677	Yes	****	<0.0001
SC (Resin) vs. Smooth (Molloplast®)	1.153	0.8445 to 1.461	Yes	****	<0.0001
SC (Resin) vs. Fixodent®	-0.0294	-0.3375 to 0.2787	No	ns	>0.9999
SC-EX (Resin) vs. Smooth (Resin)	1.318	1.010 to 1.626	Yes	****	<0.0001
SC-EX (Resin) vs. SC (Molloplast®)	1.973	1.665 to 2.281	Yes	****	<0.0001
SC-EX (Resin) vs. SC-EX (Molloplast®)	1.783	1.475 to 2.091	Yes	****	<0.0001
SC-EX (Resin) vs. Smooth (Molloplast®)	1.567	1.259 to 1.875	Yes	****	<0.0001
SC-EX (Resin) vs. Fixodent®	0.3846	0.07654 to 0.6927	Yes	**	0.0051
Smooth (Resin) vs. SC (Molloplast®)	0.6548	0.3467 to 0.9629	Yes	****	<0.0001
Smooth (Resin) vs. SC-EX (Molloplast®)	0.4644	0.1563 to 0.7725	Yes	***	0.0003
Smooth (Resin) vs. Smooth (Molloplast®)	0.2484	-0.05966 to 0.5565	No	ns	0.1996
Smooth (Resin) vs. Fixodent®	-0.9336	-1.242 to -0.6255	Yes	****	<0.0001
SC (Molloplast®) vs. SC-EX (Molloplast®)	-0.1904	-0.4985 to 0.1177	No	ns	0.5138
SC (Molloplast®) vs. Smooth (Molloplast®)	-0.4064	-0.7145 to -0.09834	Yes	**	0.0025
SC (Molloplast®) vs. Fixodent®	-1.588	-1.896 to -1.280	Yes	****	<0.0001
SC-EX (Molloplast®) vs. Smooth (Molloplast®)	-0.216	-0.5241 to 0.09206	No	ns	0.3568
SC-EX (Molloplast®) vs. Fixodent®	-1.398	-1.706 to -1.090	Yes	****	<0.0001
Smooth (Molloplast®) vs. Fixodent®	-1.182	-1.490 to -0.8739	Yes	****	<0.0001

Preload 17N					
SC (Resin) vs. SC-EX (Resin)	-0.6366	-0.9447 to -0.3285	Yes	****	<0.0001
SC (Resin) vs. Smooth (Resin)	0.9963	0.6883 to 1.304	Yes	****	<0.0001
SC (Resin) vs. SC (Molloplast®)	1.494	1.186 to 1.802	Yes	****	<0.0001
SC (Resin) vs. SC-EX (Molloplast®)	1.256	0.9479 to 1.564	Yes	****	<0.0001
SC (Resin) vs. Smooth (Molloplast®)	0.818	0.5099 to 1.126	Yes	****	<0.0001
SC (Resin) vs. Fixodent®	0.514	0.2059 to 0.8221	Yes	****	<0.0001
SC-EX (Resin) vs. Smooth (Resin)	1.633	1.325 to 1.941	Yes	****	<0.0001
SC-EX (Resin) vs. SC (Molloplast®)	2.131	1.823 to 2.439	Yes	****	<0.0001
SC-EX (Resin) vs. SC-EX (Molloplast®)	1.893	1.585 to 2.201	Yes	****	<0.0001
SC-EX (Resin) vs. Smooth (Molloplast®)	1.455	1.147 to 1.763	Yes	****	<0.0001
SC-EX (Resin) vs. Fixodent®	1.151	0.8425 to 1.459	Yes	****	<0.0001
Smooth (Resin) vs. SC (Molloplast®)	0.4977	0.1896 to 0.8057	Yes	****	<0.0001
Smooth (Resin) vs. SC-EX (Molloplast®)	0.2597	-0.04840 to 0.5677	No	ns	0.1584
Smooth (Resin) vs. Smooth (Molloplast®)	-0.1783	-0.4864 to 0.1297	No	ns	0.5921
Smooth (Resin) vs. Fixodent®	-0.4823	-0.7904 to -0.1743	Yes	***	0.0001
SC (Molloplast®) vs. SC-EX (Molloplast®)	-0.238	-0.5461 to 0.07006	No	ns	0.2439
SC (Molloplast®) vs. Smooth (Molloplast®)	-0.676	-0.9841 to -0.3679	Yes	****	<0.0001
SC (Molloplast®) vs. Fixodent®	-0.98	-1.288 to -0.6719	Yes	****	<0.0001
SC-EX (Molloplast®) vs. Smooth (Molloplast®)	-0.438	-0.7461 to -0.1299	Yes	***	0.0008
SC-EX (Molloplast®) vs. Fixodent®	-0.742	-1.050 to -0.4339	Yes	****	<0.0001
Smooth (Molloplast®) vs. Fixodent®	-0.304	-0.6121 to 0.004062	No	ns	0.0556

**Table S4. Statistical analysis and Tukey's multiple comparisons tests for dentures' detachment forces across different preloads in the environment with artificial saliva.**

### MOIST ENVIRONEMENT (KERATIN)

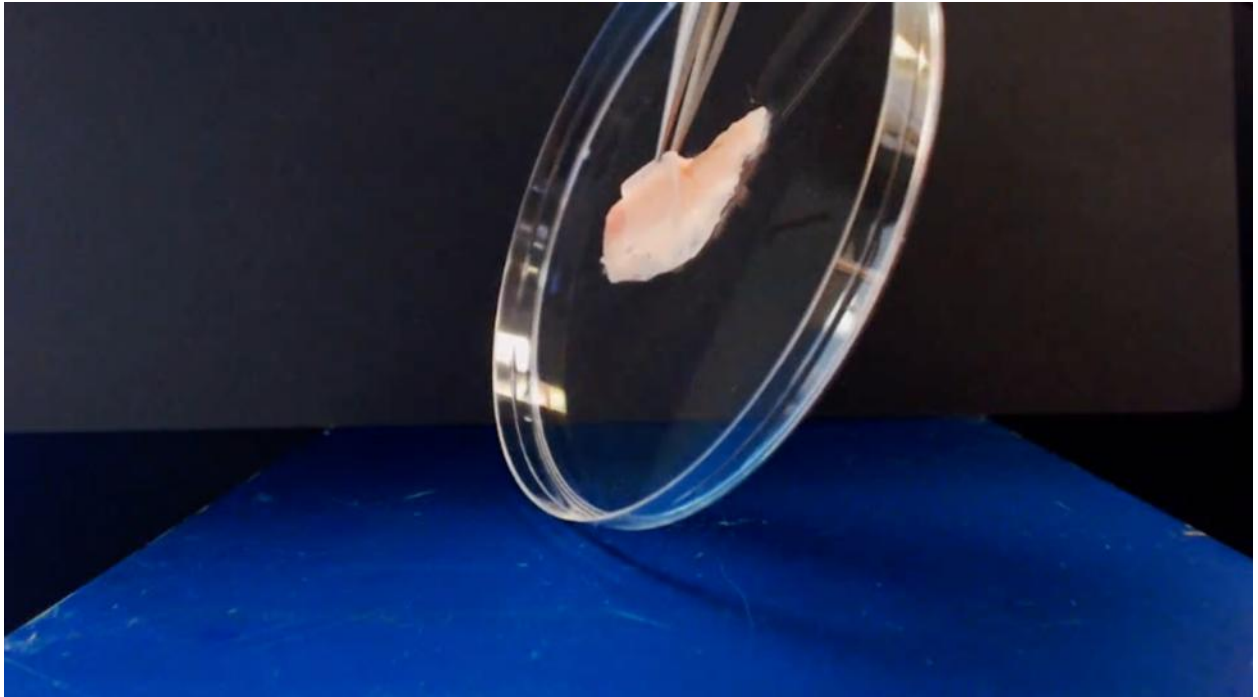
Tukey's multiple comparisons test	Mean Diff.	95.00% CI of diff.	Below threshold?	Summary	Adjusted P Value
Preload 1N					
SC (Resin+keratin) vs. SC-EX (Resin+keratin)	0.08615	-0.2020 to 0.3743	No	ns	0.8593
SC (Resin+keratin) vs. Smooth (Resin+keratin)	-0.6309	-0.9190 to -0.3428	Yes	****	<0.0001
SC (Resin+keratin) vs. Fixodent®	-1.258	-1.546 to -0.9700	Yes	****	<0.0001
SC-EX (Resin+keratin) vs. Smooth (Resin+keratin)	-0.7171	-1.005 to -0.4289	Yes	****	<0.0001
SC-EX (Resin+keratin) vs. Fixodent®	-1.344	-1.632 to -1.056	Yes	****	<0.0001
Smooth (Resin+keratin) vs. Fixodent®	-0.6272	-0.9153 to -0.3391	Yes	****	<0.0001

Preload 4N					
SC (Resin+keratin) vs. SC-EX (Resin+keratin)	-0.06235	-0.3505 to 0.2258	No	ns	0.9404
SC (Resin+keratin) vs. Smooth (Resin+keratin)	-0.5767	-0.8648 to -0.2885	Yes	****	<0.0001
SC (Resin+keratin) vs. Fixodent®	-1.355	-1.643 to -1.067	Yes	****	<0.0001
SC-EX (Resin+keratin) vs. Smooth (Resin+keratin)	-0.5143	-0.8024 to -0.2262	Yes	****	<0.0001
SC-EX (Resin+keratin) vs. Fixodent®	-1.293	-1.581 to -1.005	Yes	****	<0.0001
Smooth (Resin+keratin) vs. Fixodent®	-0.7785	-1.067 to -0.4904	Yes	****	<0.0001

Preload 10N					
SC (Resin+keratin) vs. SC-EX (Resin+keratin)	-0.2036	-0.4917 to 0.08452	No	ns	0.2538
SC (Resin+keratin) vs. Smooth (Resin+keratin)	-0.9858	-1.274 to -0.6977	Yes	****	<0.0001
SC (Resin+keratin) vs. Fixodent®	-1.448	-1.736 to -1.160	Yes	****	<0.0001
SC-EX (Resin+keratin) vs. Smooth (Resin+keratin)	-0.7822	-1.070 to -0.4941	Yes	****	<0.0001
SC-EX (Resin+keratin) vs. Fixodent®	-1.245	-1.533 to -0.9564	Yes	****	<0.0001
Smooth (Resin+keratin) vs. Fixodent®	-0.4623	-0.7504 to -0.1741	Yes	***	0.0004

Preload 17N					
SC (Resin+keratin) vs. SC-EX (Resin+keratin)	-0.2696	-0.5577 to 0.01856	No	ns	0.0748
SC (Resin+keratin) vs. Smooth (Resin+keratin)	-1.021	-1.309 to -0.7326	Yes	****	<0.0001
SC (Resin+keratin) vs. Fixodent®	-0.9066	-1.195 to -0.6184	Yes	****	<0.0001
SC-EX (Resin+keratin) vs. Smooth (Resin+keratin)	-0.7512	-1.039 to -0.4630	Yes	****	<0.0001
SC-EX (Resin+keratin) vs. Fixodent®	-0.637	-0.9251 to -0.3489	Yes	****	<0.0001
Smooth (Resin+keratin) vs. Fixodent®	0.1142	-0.1740 to 0.4023	No	ns	0.7236

**Table S5. Statistical analysis and Tukey's multiple comparisons tests for dentures' detachment forces across different preloads in moist environment with keratin.**

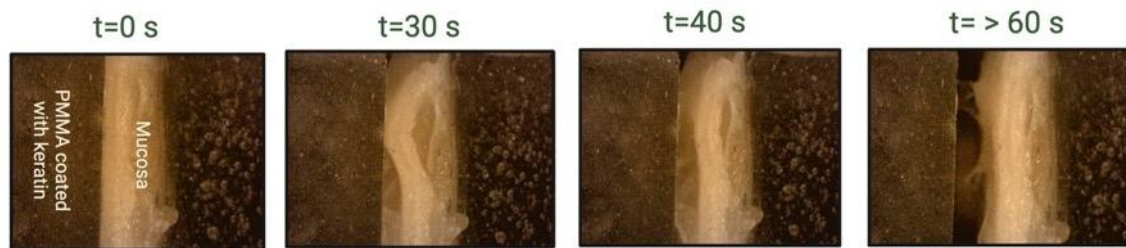


**Movie S1. Keratin-coated acrylic block and its interaction with the keratinized mucosa.**

Example of keratin-coated acrylic block withstanding the attempts to break the joint established at the interface between mucosa and the acrylic block.

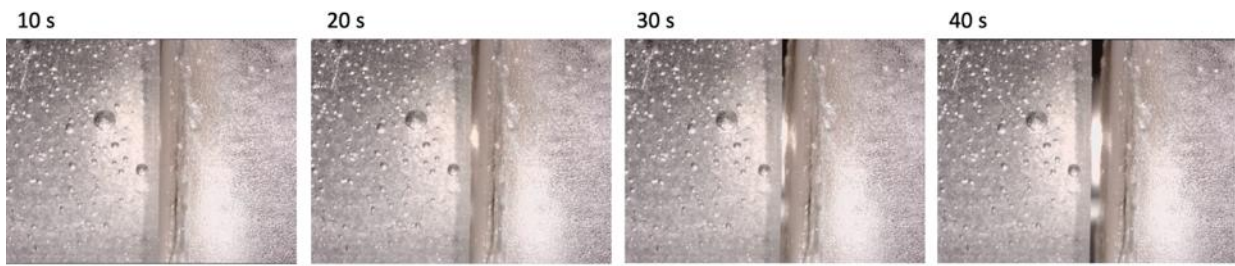


**Movie S2. Non-coated acrylic block and its interaction with the keratinized mucosa. The acrylic block could be easily detached from the surface.**



**Movie S3. An example of a keratin-coated acrylic block being pulled away from the surface of keratinized mucosa and observed under a microscope while using a micro tensile tester. Microstrings are visualized after 40 s of retraction.**

The captions in Figure 3e of the main text correspond to the extended version of this video, which explains the differences in the timeframes stated above the images.



**Movie S4. An example of the non-coated acrylic block being pulled away from the surface of keratinized mucosa and observed under a microscope while using a micro tensile tester. Microstrings were not visualized during the retraction.**